Imaging Techniques in Insects

Marco Paoli, Mara Andrione, Albrecht Haase

Neuromethods 217

Springer Protocols

Lesley J. Rogers
Giorgio Vallortigara *Editors*

Lateralized Brain Functions

Methods in Human and Non-Human Species

Second Edition

Humana Press

NEUROMETHODS

Series Editor
Wolfgang Walz
University of Saskatchewan
Saskatoon, SK, Canada

For further volumes:
http://www.springer.com/series/7657

Neuromethods publishes cutting-edge methods and protocols in all areas of neuroscience as well as translational neurological and mental research. Each volume in the series offers tested laboratory protocols, step-by-step methods for reproducible lab experiments and addresses methodological controversies and pitfalls in order to aid neuroscientists in experimentation. *Neuromethods* focuses on traditional and emerging topics with wide-ranging implications to brain function, such as electrophysiology, neuroimaging, behavioral analysis, genomics, neurodegeneration, translational research and clinical trials. *Neuromethods* provides investigators and trainees with highly useful compendiums of key strategies and approaches for successful research in animal and human brain function including translational "bench to bedside" approaches to mental and neurological diseases.

Lateralized Brain Functions

Methods in Human and Non-Human Species

Second Edition

Edited by

Lesley J. Rogers

School of Science and Technology, University of New England, Armidale, NSW, Australia

Giorgio Vallortigara

Center for Mind/Brain Sciences, University of Trento, Rovereto, TN, Italy

Humana Press

Editors
Lesley J. Rogers
School of Science and Technology
University of New England
Armidale, NSW, Australia

Giorgio Vallortigara
Center for Mind/Brain Sciences
University of Trento
Rovereto, TN, Italy

ISSN 0893-2336 ISSN 1940-6045 (electronic)
Neuromethods
ISBN 978-1-0716-4239-9 ISBN 978-1-0716-4240-5 (eBook)
https://doi.org/10.1007/978-1-0716-4240-5

This Humana imprint is published by the registered company Springer Science+Business Media, LLC, part of Springer Nature.
The registered company address is: 1 New York Plaza, New York, NY 10004, U.S.A.

Preface

We ended the preface of the first edition with the hope that this book would develop the field to such an extent that it would lead to a need for a second edition, covering a new collection of methods. And, in fact, eight years later we are here to present a new edition, with many important innovations.

The early discovery of structural asymmetry in the nervous systems of non-human animals dates back to the neuroanatomical studies on diencephalic structures carried out on fish and amphibians between 1900 and 1930 (see [1] for a historical account). Yet, it was with evidence for functional lateralization, made in two avian species and rats in the 1970s and early 1980s [2–4], that investigation of lateralization in non-human species exploded, developing into a stream of publications on laterality in different species, both vertebrates [5–8] and invertebrates [9].

The availability of animal models for studying lateralization has produced two important changes. Firstly, it has promoted a resurgence of interest in a research area that previously had been confined to human neuropsychology and neurology and had shown signs of declining interest because it appeared to be incapable of tackling the most basic issues; namely, the causes of lateralization of the brain and its biological function [10]. The entering of animal biology into the study of lateralization has not only brought about the availability of new system models with better accessibility to neural structures and functions but also it has provided a different way of considering the origins and biological significance of lateralization in evolutionary terms [11]. In this regard, for example, theoretical tools from game theory and population genetics have prompted unexpected advances in our understanding of the evolution of brain asymmetry [12–15].

The second important change allowed scientists to develop and use new techniques for studying brain and behavioral lateralization. In addition, it is recognized that these animal models are potentially able to enhance understanding of individual differences in behavior and aberrant behavioral and neural conditions in humans, as well as in non-human species [16–18]. Many different experimental approaches have been applied, each adapted to reveal lateralization in different species or to do so more precisely in species already known to be lateralized. This has led to a broad range of techniques with varying success in revealing lateralization of both brain function and brain structure. Nowadays, novel themes have been added (or re-discovered) to the traditional topics associated with the study of brain asymmetry, including the different phenotypic appearances of asymmetries [19] with their clinical relevance [20], or the genetic bases of laterality (e.g., [21] and Chapters 18 and 19).

Research in the area of neuroscience of lateralization in humans has also progressed in recent years, and neuroimaging and neurostimulation techniques have become a source of new data on lateralization. Interestingly, the development of techniques to be used with animal model systems has also had an influence on research of lateralization in humans. An example is provided by the ethological methods developed to investigate lateralization in everyday behavior in non-human species, methods that are now used widely in humans as well [22, 23].

The issue of the evolutionary origins of lateralization is still captivating attention [11, 24–25], and to the traditional models based on population dynamics [26, 27] some new approaches based on free energy minimization have been added [28]. Intriguingly, the

observation of asymmetries in eye use in animals with eyes positioned laterally on the sides of their head, and with few inter-hemispheric connections, has been rekindled (Chapter 3) and provided novel impetus to the philosophical issue of whether a split-brain condition could give rise to two minds within one body (e.g., [29]).

The focus of this book remains, however, up-to-date coverage of the new techniques used to study brain and behavioral laterality in both human and non-human animals. The different experimental approaches that have been described have all been updated and some new chapters have been added (Chapters 4 and 13). One new chapter reports behavioral measurements based on occlusion of one eye in birds (Chapter 4). The development of new techniques of computational ethology (e.g., [30]) promises to impact the study of lateralized behavior in animals in important ways [31, 32]. The other new chapter is related to imaging techniques that allow direct scrutiny of brain activity in embryos (Chapter 13), which is providing evidence for brain activity and connectivity modulated by environmental stimulation [33], a factor shown to be crucial in the development of lateralization ([34, 35]; Chapter 21).

New methods developed to test different species need to take into account species differences in sensory and motor systems. Study of several vertebrate species has led to the realization that a basic pattern of asymmetry of functions is common across vertebrate species [36]. The right hemisphere is specialized to attend to novel stimuli, including predators, to control social behavior, recognize faces, and process global information using spatial cues [37]. The left hemisphere is specialized for focused attention needed to perform learned tasks, to follow rules, and to categorize stimuli [6]. This division of functions is present in humans also [35].

Important to understanding lateralization is knowledge of how it develops in humans [38, 39] and other species [40]. A few key nonhuman species have been the focus of detailed study of development, including domestic chicks [41–43], pigeons [44], and zebrafish [45–48]. These species were chosen as models for studying the development of lateralization because their stages of development are known rather precisely and because sensory inputs can be manipulated with the aim of determining the role of sensory experience in the development of lateralization. In all these species, there is clear evidence that exposing the developing embryo to light is essential for the development of visual lateralization. For example, light exposure of avian embryos during the final stages of development before hatching stimulates the right eye but not the left eye because the embryo's head is twisted to the side so that the left eye is occluded by the embryo's body [50]. This difference in stimulation of the left and right eyes at a time when connections between eye and brain first become functional is essential in establishing certain visual lateralities, known because these functions are not lateralized if the embryos are incubated in the dark during this critical stage of development [50–51]. Light stimulation at this stage of embryonic development also has asymmetrical effects on neural responsiveness in the Wulst region of the forebrain [52]. Furthermore, light exposure prior to this stage of embryonic development also influences laterality after hatching ([53] and see Chapter 21).

Of course, detailed knowledge of the function of lateralization is essential. What are the advantages of having a lateralized brain and, on the contrary, what disadvantages might be apparent? In this aspect of investigation, it is important to consider two distinct types of lateralization: individual and population lateralization [24]. Individual lateralization is that present in individual members of a species but it may favor the left side in some individuals and the right side in others, leading to no directional bias within the group or population.

Population lateralization, also referred to as directional lateralization, is present when most individuals are lateralized in the same direction. Handedness in humans is an example of the latter, as also is the lateralization of visual processing in birds that we have discussed above.

This edition has some chapters with methods that are simple to apply and others that require more sophisticated techniques, often newly available. Each set of methods can lead to discovery of different levels or types of lateralization and, contrary to one approach superseding another, all methods can be complementary in advancing understanding. Every chapter covers the latest evidence and techniques applied in its area.

Chapters 1, 2, 3, 4, 5, 6, and 7 include the methods of measuring lateralization in a range of species by scoring behavior elicited by inputs to one or the other side of the brain. These chapters include some of the classic methods developed by experimental psychologists to deal with hemispheric specialization, such as tachistoscopic viewing and dichotic listening (Chapter 1 by Ocklenburg), which have been improved to higher levels of technical precision and sophistication, or the study of split-brain patients of the clinical neuropsychological tradition (Chapter 2 by Fabri, Foschi, Pierpaoli, and Polonara). The roots of all these methods can be traced back to the early sensory physiology and psychology of the nineteenth century. In fact, it was Gustav Fechner, the founder of psychophysics, who made the first inquiry about the possible outcome of disconnecting the two cerebral hemispheres: "The two cerebral hemispheres, while beginning with the same moods, predispositions, knowledge, and memories, indeed the same consciousness generally, will [when divided through the middle] thereafter develop differently according to the external relations into which each will enter" (Gustav Theodor Fechner, 1860, in Zangwill [54]).

New methods have come from ethology and include measurements of eye preferences (particularly in animals with laterally placed eyes and complete decussation at the optic chiasma) and ear preferences (Chapter 3 by Rogers and an entirely new Chapter 4 by Rosa-Salva and Vallortigara), as well as preferences in nostril use and olfactory stimulation (Chapter 5 by Siniscalchi). Behavioral methods have been developed to study motor preferences (Chapter 6 by Malatesta and Forrester) and lateralization in invertebrates (Chapter 7 by Liga and Frasnelli). Thanks to the limited number of neurons of invertebrate species, the combination of behavioral analyses with sophisticated molecular and genetic techniques available for species such as the fruitfly may provide important breakthroughs in the study of brain asymmetries. In fact, the study of hand and limb preferences, which has been traditionally the province of an allegedly unique phenomenon, i.e., human handedness, has been deeply challenged by the mounting evidence from studies on non-human primates and other species, both mammals and birds [55, 56], showing a variety of asymmetries in limb usage. Here the availability of precise techniques of recording use of the limbs in natural and semi-natural conditions may prove crucial in comparing in a proper way strength and direction of handedness in different species (Chapter 6 by Malatesta and Forrester).

Chapters 8, 9, 10, 11, and 12 cover neurobiological methods used to reveal lateralization. Again, these include both well-established techniques such as lesion studies (Chapter 8 by Manns), electrophysiological and pharmacological techniques (Chapter 9 by McCabe), tract tracing (Chapter 10 by Stöckens and Güntürkün), and early gene expression (Chapter 11 by Patton, Uysal, Kellog, and Shimizu), as well as advances in understanding the role of steroid hormones in expression of lateralization (Chapter 12 by Beking, Geuze, and Groothuis).

Chapters 13, 14, 15, 16, and 17 discuss imaging techniques, electroencephalographic techniques and transcranial stimulation used to reveal lateralization. The mixture of human and non-human animal research here is apparent, with non-invasive techniques, such as the

new technique of imaging asymmetrical brain activity in embryos (Chapter 13 by Cavallari, Bifore, Vallortigara, and Lorenzi) and transcranial magnetic stimulation (Chapter 14 by Cattaneo) and electroencephalographic stimulation (Chapter 15 by Asseconi, Pagno, and Mazza) mainly used for research in humans, fMRI imaging used to compare human and non-human primates species (Chapter 16 by Hopkins and Phillips), and other more recent methods with much finer spatial and temporal resolution, such as two-photon microscopy, confined at present to system models such as insects (Chapter 17 by Paoli, Andrione, and Haase).

New genetic techniques used to study lateralization in humans (Chapter 18 by Paracchini) and zebrafish (Chapter 19 by Ariyasiri, Cheng and Halpern) are powerful ways of addressing the role of genes in the establishment and development of brain asymmetry. Last but by no means least are two chapters covering methods used to study the development of lateralization. Chapter 20 by Blackiston and Levin covers model systems for the study of lateralized development and Chapter 21 by Chiandetti provides the readers with updated information about changes in lateralization that occur by manipulating sensory exposure.

We believe that this collection of revised and new chapters will provide a strong basis for further research on brain and behavioral asymmetries in human and non-human species. In particular, we hope this book will contribute to bridging the gap between laterality research in human subjects and non-human model species. Exciting new data are emerging that relate brain asymmetries to epigenetic events in humans (e.g., neurons of the human prefrontal cortex exhibit higher DNA methylation levels in the left hemisphere compared to those of the right hemisphere [57]). However, epigenetic effects are tested with bio-assays that are tissue-specific and time-sensitive, e.g., histone modification; thus, comparative research in animal model species will be crucial in order to produce advancements in this field. This book will, we hope, shape the next decade of laterality research by opening the way for novel questions and enhancing collaborations.

Armidale, NSW, Australia — *Lesley J. Rogers*
Rovereto, Italy — *Giorgio Vallortigara*

References

1. Braitenberg V, Kemali M (1970) Exceptions to bilateral symmetry in the epithalamus of lower vertebrates. J Comp Neurol 138:137–146
2. Nottebohm F (1971) Neural lateralization of vocal control in a passerine bird. I. Song. J Exp Zool 177: 229–261
3. Rogers LJ, Anson JM (1979) Lateralisation of function in the chicken forebrain. Pharmacol Biochem Behav 10:679–686
4. Denenberg VH (1981) Hemispheric laterality in animals and the effects of early experience. Behav Brain Sci 4:1–49
5. Vallortigara G (2000) Comparative neuropsychology of the dual brain: a stroll through left and right animals' perceptual worlds. Brain Lang 73:189–219
6. Rogers LJ, Vallortigara G, Andrew RJ (2013) Divided brains: the biology and behaviour of brain asymmetries. Cambridge University Press, Cambridge
7. Stancher G, Sovrano VA, Vallortigara G (2018) Motor asymmetries in fishes, amphibians and reptiles, in 'Cerebral lateralization and cognition: evolutionary and developmental investigations of behavioral biases'. Prog Brain Res 238:35–56
8. Petrazzini ME, Sovrano VA, Vallortigara G, Messina A (2020) Brain and behavioral asymmetry: a lesson from fish. Front Neuroanat 14:11. https://doi.org/10.3389/fnana.2020.00011

9. Frasnelli E, Vallortigara G, Rogers LJ (2012) Left-right asymmetries of behaviour and nervous system in invertebrates. Neurosci Biobehav Rev 36:1273–1291
10. Efron R (1990) The decline and fall of hemispheric specialization. Lawrence Erlbaum Associates, Hillsdale
11. Rogers LJ, Vallortigara G (2015) When and why did brains break symmetry? Symmetry 7:2181–2194
12. Ghirlanda S, Frasnelli E, Vallortigara G (2009) Intraspecific competition and coordination in the evolution of lateralization. Philos Trans R Soc Lond B Biol Sci 364:861–866
13. Ghirlanda S, Vallortigara G (2004) The evolution of brain lateralization: a game theoretical analysis of population structure. Proc Biol Sci 271:853–857
14. Raymond M, Pontier D, Dufour AB, Moller A (1996) Frequency-dependent maintenance of left handedness in humans. Proc R Soc Lond B 263:1627–1633. https://doi.org/10.1098/rspb.1996.0238
15. Vallortigara G (2006) The evolutionary psychology of left and right: costs and benefits of lateralization. Dev Psychobiol 48:418–427. https://doi.org/10.1002/dev.20166
16. Concha ML, Bianco IH, Wilson SW (2012) Encoding asymmetry within neural circuits. Nat Rev Neurosci 13:832–843
17. Duboc V, Dufourcq P, Blader P, Roussingé M (2015) Asymmetry of the brain: development and implications. Annu Rev Genet 49:26.1–26.26
18. Branson NJ, Rogers LJ (2006) Relationship between paw preference strength and noise phobia in *Canis familiaris*. J Comp Psychol 120(3):176–183
19. Ocklenburg S, Mundorf A, Gerrits R et al (2024) Clinical implications of brain asymmetries. Nat Rev Neurol. https://doi.org/10.1038/s41582-024-00974-8
20. Vingerhoets G (2019) Phenotypes in hemispheric functional segregation? Perspectives and challenges. Phys Life Rev Jul 29. pii: S1571-0645(19)30104-6. https://doi.org/10.1016/j.plrev.2019.07.008
21. Powell GT et al (2024) Cachd1 interacts with Wnt receptors and regulates neuronal asymmetry in the zebrafish brain. Science 384:573–579. https://doi.org/10.1126/science.ade6970
22. Forrester GS, Pegler R, Thomas MA, Mareschal D (2014) Handedness as a marker of cerebral lateralization in children with and without autism. Behav Brain Res 268:14–21
23. Marzoli D, Tommasi L (2009) Side biases in humans (*Homo sapiens*): three ecological studies on hemispheric asymmetries. Naturwissenschaften 96(9):1099–1106
24. Vallortigara G, Rogers LJ (2005) Survival with an asymmetrical brain: advantages and disadvantages of cerebral lateralization. Behav Brain Sci 28:575–589
25. Güntürkün O, Strökens F, Ocklenburg S (2020) Brain lateralization: a comparative perspective. Physiol Rev 100:1019–1063. https://doi.org/10.1152/physrev.00006.2019
26. Ghirlanda S, Vallortigara G (2004) The evolution of brain lateralization: a game theoretical analysis of population structure. Proc Biol Sci 271:853–857
27. Abrams DM, Panaggio MJ (2012) A model balancing cooperation and competition can explain our right-handed world and the dominance of left-handed athletes. J R Soc Interface 9:2718–2722. https://doi.org/10.1098/rsif.2012.0211
28. Vallortigara G, Vitiello G (2024) Brain asymmetry as minimization of free energy: a theoretical model. R Soc Open Sci 11(7):240465
29. Godfrey-Smith P (2021) Integration, lateralization, and animal experience. Mind Lang 36:285–296
30. Zanon M, Lemaire BS, Vallortigara G (2021) Steps towards a computational ethology: an automatized, interactive setup to investigate filial imprinting and biological predispositions. Biol Cybern 115(6):575–584. https://doi.org/10.1007/s00422-021-00886-6
31. Josserand M, Rosa-Salva O, Versace E, Lemaire BS (2022) Visual field analysis: a reliable method to score left and right eye use using automated tracking. Behav Res Methods 54:1715–1724. https://doi.org/10.3758/s13428-021-01702-6
32. Vallortigara G (2021) Laterality for the next decade: computational ethology and the search for minimal condition for cognitive asymmetry. Laterality 26(3):303–306. https://doi.org/10.1080/1357650X.2020.1870122
33. Lorenzi E, Tambalo S, Vallortigara G, Bifone A (2023) Manganese-enhanced magnetic resonance imaging reveals light-induced brain asymmetry in embryo. eLife 12:e86116. https://doi.org/10.7554/eLife.86116

34. Rogers LJ (2023) Unfolding a sequence of sensory influences and interactions in the development of functional brain laterality. Front Behav Neurosci 16:1103192. https://doi.org/10.3389/fnbeh.2022.1103192
35. Vallortigara G, Rogers LJ (2020) A function for the bicameral mind. Cortex 124:274–285. https://doi.org/10.1016/j.cortex.2019.11.018
36. MacNeilage PF, Rogers LJ, Vallortigara G (2009) Origins of the left and right brain. Sci Am 301:60–67
37. Rosa Salva O, Regolin L, Mascalzoni E, Vallortigara G (2012) Cerebral and behavioural asymmetry in animal social recognition. Comp Cogn Behav Rev 7:110–138. https://doi.org/10.3819/ccbr.2012.70006
38. Michel GF (2021) Handedness development: a model for investigating development of hemispheric specialization and hemispheric coordination. Symmetry 13:992. https://doi.org/10.3390/sym13060992
39. Nelson EL, Gonzalez SL, Coxe S, Campbell JM, Marcinowski EC, Michel GF (2017) Toddler hand preference trajectories predict 3-year language outcome. Dev Psychobiol 59:876–887. https://doi.org/10.1002/dev.21560
40. Nelson EL (2022) Developmental cascades as a framework for primate handedness. Front Behav Neurosci 16:1063348. https://doi.org/10.3389/fnbeh.2022.1063348
41. Andrew RJ (1991) The nature of behavioral lateralization in the chick. In: In Andrew RJ (ed) Neural and behavioral plasticity, The use of the Chick as a Model. Oxford University Press, Oxford, pp 536–554
42. Vallortigara G, Cozzutti C, Tommasi L, Rogers LJ (2001) How birds use their eyes: opposite left-right specialisation for the lateral and frontal visual hemifield in the domestic chick. Curr Biol 11:29–33
43. Rogers LJ (1996) Behavioral, structural and neurochemical asymmetries in the avian brain: a model system for studying visual development and processing. Neurosci Biobehav Rev 20:487–503
44. Güntürkün O (2006) Avian cerebral asymmetries: the view from the inside. Cortex 42:104–106
45. Barth KA, Miklosi A, Watkins J, Bianco IH, Wilson SW, Andrew RJ (2005) fsi zebrafish show concordant reversal of viscera, neuroanatomy and subset of behavioural responses. Curr Biol 15:844–850
46. Concha ML, Burdine RD, Russell C, Schier AF, Wilson SW (2000) A nodal signaling pathway regulates the laterality of neuroanatomical asymmetries in the zebrafish forebrain. Neuron 28:399–409
47. Gamse JT, Thisse C, Thisse B, Halpern ME (2003) The parapineal mediates left-right asymmetry in the zebrafish diencephalons. Development 130:1059–1068
48. Sovrano VA, Andrew RJ (2006) Eye use during viewing a reflection: behavioural lateralisation in zebrafish larvae. Behav Brain Res 167(2):226–231
49. Rogers LJ, Andrew RJ (eds) (2002) Comparative vertebrate lateralization. Cambridge University Press, Cambridge
50. Rogers LJ (1990) Light input and the reversal of functional lateralization in the chicken brain. Behav Brain Res 38:211–221
51. Rogers LJ (1982) Light experience and asymmetry of brain function in chickens. Nature 297:223–225. https://doi.org/10.1038/297223a0
52. Costalunga G, Kobylkov D, Rosa-Salva O, Vallortigara G, Mayer U (2022) Light-incubation effects on lateralisation of single unit responses in the visual Wulst of domestic chicks. Brain Struct Funct 227(2):497–513. https://doi.org/10.1007/s00429-021-02259-y
53. Chiandetti C, Lemaire BS, Versace E, Vallortigara G (2017) Early- and late-light embryonic stimulation modulates similarly chicks' ability to filter out distractors. Symmetry 9:84. https://doi.org/10.3390/sym9060084
54. Zangwill OL (1974) Consciousness and the cerebral hemispheres. In: Dimond SJ, Beaumont, JG (eds) Hemispheric function in the human brain. Wiley, New York. pp.264-278
55. Versace E, Vallortigara G (2015) Forelimb preferences in human beings and other species: multiple models for testing hypotheses on lateralization. Front Psychol 6:233. https://doi.org/10.3389/fpsyg.2015.00233
56. Kaplan G, Rogers LJ (2021) Brain size associated with foot preferences in Australian parrots. Symmetry 13:867. https://doi.org/10.3390/sym13050867
57. Li P, Ensink E, Lang S, Marshall L, Schilthuis M, Lamp J et al (2020) Hemispheric asymmetry in the human brain and in Parkinson's disease is linked to divergent epigenetic patterns in neurons. Genome Biol 21(1):1–23

Preface to the Series

Experimental life sciences have two basic foundations: concepts and tools. The Neuromethods series focuses on the tools and techniques unique to the investigation of the nervous system and excitable cells. It will not, however, shortchange the concept side of things as care has been taken to integrate these tools within the context of the concepts and questions under investigation. In this way, the series is unique in that it not only collects protocols but also includes theoretical background information and critiques which led to the methods and their development. Thus it gives the reader a better understanding of the origin of the techniques and their potential future development. The Neuromethods publishing program strikes a balance between recent and exciting developments like those concerning new animal models of disease, imaging, in vivo methods, and more established techniques, including, for example, immunocytochemistry and electrophysiological technologies. New trainees in neurosciences still need a sound footing in these older methods in order to apply a critical approach to their results.

Under the guidance of its founders, Alan Boulton and Glen Baker, the Neuromethods series has been a success since its first volume published through Humana Press in 1985. The series continues to flourish through many changes over the years. It is now published under the umbrella of Springer Protocols. While methods involving brain research have changed a lot since the series started, the publishing environment and technology have changed even more radically. Neuromethods has the distinct layout and style of the Springer Protocols program, designed specifically for readability and ease of reference in a laboratory setting.

The careful application of methods is potentially the most important step in the process of scientific inquiry. In the past, new methodologies led the way in developing new disciplines in the biological and medical sciences. For example, Physiology emerged out of Anatomy in the nineteenth century by harnessing new methods based on the newly discovered phenomenon of electricity. Nowadays, the relationships between disciplines and methods are more complex. Methods are now widely shared between disciplines and research areas. New developments in electronic publishing make it possible for scientists that encounter new methods to quickly find sources of information electronically. The design of individual volumes and chapters in this series takes this new access technology into account. Springer Protocols makes it possible to download single protocols separately. In addition, Springer makes its print-on-demand technology available globally. A print copy can therefore be acquired quickly and for a competitive price anywhere in the world.

Saskatoon, SK, Canada *Wolfgang Walz*

Contents

Contributors

Mara Andrione • *Department of Neurobiology, University of Vienna, Vienna, Austria*

Krishan Ariyasiri • *Department of Molecular and Systems Biology, Geisel School of Medicine at Dartmouth, Hanover, NH, USA*

Sara Assecondi • *Center for Mind/Brain Sciences (CIMeC), University of Trento, Rovereto, TN, Italy*

Tess Beking • *Clinical and Developmental Neuropsychology and Behavioral Biology, Groningen Institute for Evolutionary Life Sciences, University of Groningen, Groningen, The Netherlands*

Angelo Bifone • *Department of Molecular Biotechnology and Health Sciences, University of Torino, Torino, Italy*

Douglas J. Blackiston • *Department of Biology, and Allen Discovery Center, Tufts University, Medford, MA, USA*

Luigi Cattaneo • *Center for Mind/Brain Sciences (CIMeC) – University of Trento, Rovereto, TN, Italy*

Eleonora Cavallari • *Department of Molecular Biotechnology and Health Sciences, University of Torino, Torino, Italy*

Ji Cheng • *Department of Molecular and Systems Biology, Geisel School of Medicine at Dartmouth, Hanover, NH, USA*

Cinzia Chiandetti • *Department of Life Sciences, University of Trieste, Trieste, Italy*

Mara Fabri • *Dipartimento di Scienze della Vita e dell'Ambiente, Università Politecnica delle Marche, Ancona, Italy*

Gillian S. Forrester • *School of Psychology, University of Sussex, Brighton, UK*

Nicoletta Foschi • *Centro Epilessia, Clinica di Neurologia, Azienda Ospedaliera-Universitaria Umberto I, Ancona, Italy*

Elisa Frasnelli • *Invertebrate and Neuroscience Group (ING), Animal Cognition and Neuroscience Laboratory, Centre for Mind/Brain Sciences, University of Trento, Rovereto, TN, Italy*

Reint H. Geuze • *Developmental and Clinical Neuropsychology, Department of Psychology, University of Groningen, Groningen, The Netherlands*

Ton G. G. Groothuis • *Behavioral Biology, Groningen Institute for Evolutionary Life Sciences, and Research School of Behavioural and Cognitive Neurosciences, University of Groningen, Groningen, The Netherlands*

Onur Güntürkün • *Institute of Cognitive Neuroscience, Biopsychology, Department of Psychology, Ruhr-University Bochum, Bochum, Germany*

Albrecht Haase • *Center for Mind/Brain Sciences (CIMeC), University of Trento, Rovereto, Italy; Department of Physics, University of Trento, Trento, Italy*

Marnie E. Halpern • *Department of Molecular and Systems Biology, Geisel School of Medicine at Dartmouth, Hanover, NH, USA*

William D. Hopkins • *Neuroscience Institute and Language Research Center, Georgia State University, Atlanta, GA, USA; Division of Developmental and Cognitive Neuroscience, Yerkes National Primate Research Center, Atlanta, GA, USA*

S. Leilani Kellogg • *Department of Psychology, University of South Florida, Tampa, FL, USA*

Michael Levin • *Department of Biology, and Allen Discovery Center, Tufts University, Medford, MA, USA*
Davide Liga • *Centre for Mind/Brain Sciences, University of Trento, Rovereto, TN, Italy*
Elena Lorenzi • *Animal Brain and Cognition Group, Centre for Mind/Brain Sciences, University of Trento, Rovereto, TN, Italy*
Gianluca Malatesta • *Department of Psychology, University "G. d'Annunzio" of Chieti-Pescara, Chieti, Italy*
Martina Manns • *Department of Psychiatry, Psychotherapy and Preventive Medicine, LWL University Hospital, Ruhr- University Bochum, Bochum, Germany*
Veronica Mazza • *Center for Mind/Brain Sciences (CIMeC), University of Trento, Rovereto, TN, Italy*
Brian McCabe • *Department of Zoology, University of Cambridge, Cambridge, UK*
Sebastian Ocklenburg • *Institute of Cognitive and Affective Neuroscience, MSH Medical School Hamburg, Hamburg, Germany*
Silvia Pagano • *Center for Mind/Brain Sciences (CIMeC), University of Trento, Rovereto, TN, Italy*
Marco Paoli • *Neuroscience Paris-Seine – Institut de biologie Paris-Seine, Sorbonne Université, INSERM, CNRS, Paris, France; Centre des Sciences du Goût et de l'Alimentation, CNRS, INRAe, Institut Agro, Université de Bourgogne, Dijon, France*
Silvia Paracchini • *School of Medicine, University of St Andrews, St Andrews, Scotland, UK*
Tadd B. Patton • *Department of Psychological Sciences, Augusta University, Augusta, GA, USA*
Kimberley A. Phillips • *Department of Psychology, Trinity University, San Antonio, TX, USA*
Chiara Pierpaoli • *UOST, Inps Casilino-Prenestino, Rome, Italy*
Gabriele Polonara • *Dipartimento di Scienze Cliniche Specialistiche e Odontostomatologiche, Sezione di Scienze Radiologiche, Università Politecnica delle Marche, Ancona, Italy*
Lesley J. Rogers • *School of Science and Technology, University of New England, Armidale, NSW, Australia*
Orsola Rosa-Salva • *Center for Mind/Brain Sciences, University of Trento, Rovereto, TN, Italy*
Toru Shimizu • *Department of Psychology, University of South Florida, Tampa, FL, USA*
Marcello Siniscalchi • *Department of Veterinary Medicine – Animal Physiology and Behaviour Unit, University of Bari "Aldo Moro", Bari, Italy*
Felix Ströckens • *Cécile & Oskar Vogt Institute of Brain Research, Medical Faculty and University Hospital Düsseldorf, Heinrich Heine University Düsseldorf, Düsseldorf, Germany*
Ahmet K. Uysal • *Department of Psychology, University of South Florida, Tampa, FL, USA*
Giorgio Vallortigara • *Center for Mind/Brain Sciences, University of Trento, Rovereto, TN, Italy; Animal Brain and Cognition Group, Centre for Mind/Brain Sciences, University of Trento, Rovereto, TN, Italy*

temporale grey matter volume asymmetries in newborn monkeys (Papio anubis). Brain Struct Funct 227(2):463–468. https://doi.org/10.1007/s00429-021-02278-9

39. Shapleske J, Rossell SL, Woodruff PW, David AS (1999) The planum temporale: a systematic, quantitative review of its structural, functional and clinical significance. Brain Res Rev 29:26–49
40. Josse G, Mazoyer B, Crivello F, Tzourio-Mazoyer N (2003) Left planum temporale: an anatomical marker of left hemispheric specialization for language comprehension. Cogn Brain Res 18:1–14
41. Li X, Crow TJ, Hopkins WD, Roberts N (2020) Comparison of surface area and cortical thickness asymmetry in the human and chimpanzee brain. Cereb Cortex. https://doi.org/10.1093/cercor/bhaa202
42. Fischl B, van der Kouwe A, Destrieux C, Halgren E, Segonne F, Salat DH et al (2004) Automatically parcellating the human cerebral cortex. Cereb Cortex 14(1):11–22. https://doi.org/10.1093/cercor/bhg087
43. Desikan RS, Segonne F, Fischl B, Quinn BT, Dickerson BC, Blacker D et al (2006) An automated labeling system for subdividing the human cerebral cortex on MRI scans into gyral based regions of interest. NeuroImage 31:968–980
44. Vickery S, Hopkins WD, Sherwood CC, Schapiro SJ, Latzman RD, Caspers S et al (2020) Chimpanzee brain morphometry utilizing standardized MRI preprocessing and macroanatomical annotations. Elife 9:e60136. https://doi.org/10.7554/eLife.60136
45. Hopkins WD, Pilcher DL, MacGregor L (2000) Sylvian fissure length asymmetries in primates revisited: a comparative MRI study. Brain Behav Evol 56:293–299
46. Cantalupo C, Pilcher D, Hopkins WD (2003) Are planum temporale and sylvian fissure asymmetries directly related? A MRI study in great apes. Neuropsychologia 41:1975–1981
47. Liu ST, Phillips KA (2009) Sylvian fissure asymmetries in capuchin monkeys (*Cebus apella*). Laterality 14(3):217–227
48. Ide A, Rodriguez E, Zaidel E, Aboitiz F (1996) Bifurcation patterns in the human sylvian fissure: hemispheric and sex differences. Cereb Cortex 6(5):717–725
49. Gilissen E (1992) The neocortical sulci of the capuchin monkey (Cebus): evidence for asymmetry in the sylvian sulcus and comparison with other primates. Comptes Rendus de l'Academie de Sciences Paris, Series III 314: 165–170
50. Gilissen E (2001) Structural symmetries and asymmetries in human and chimpanzee brains. In: Falk D, Gibson KR (eds) Evolutionary anatomy of the primate cerebral cortex. Cambridge University, Cambridge, pp 187–215
51. Yeni-Komshian GH, Benson DA (1976) Anatomical study of cerebral asymmetry in the temporal lobe of humans, chimpanzees, and rhesus monkeys. Science 192(4237): 387–389. https://doi.org/10.1126/science.816005
52. Kochunov PV, Mangin JF, Coyle T, Lancaster JL, Thompson P, Riviere D et al (2005) Age-related morphology trends in cortical sulci. Hum Brain Mapp 26(3):210–220
53. Autrey MM, Reamer LA, Mareno MC, Sherwood CC, Herndon JG, Preuss TM et al (2014) Age-related effects in the neocortical organization of chimpanzees: gray and white matter volume, cortical thickness, and gyrification. NeuroImage 101:59–67
54. Kochunov PV, Glahn DC, Fox PT, Lancaster JL, Saleem KS, Shelledy W et al (2010) Genetics of primary cerebral gyrification: heritability of length, depth and area of primary sulci in an extended pedigree of Papio baboons. NeuroImage 53(3):1126–1134
55. Rogers J, Kochunov PV, Lancaster JL, Sheeledy W, Glahn D, Blangero J, Fox PT (2007) Heritability of brain volume, surface area and shape: an MRI study in an extended pedigree of baboons. Hum Brain Mapp 28: 576–583
56. Rogers J, Kochunov PV, Zilles K, Shelledy W, Lancaster JL, Thompson P et al (2010) On the genetic architecture of cortical folding and brain volume in primates. NeuroImage 53: 1103–1108
57. Hopkins WD, Meguerditchian A, Coulon O, Bogart SL, Mangin JF, Sherwood CC et al (2014) Evolution of the central sulcus morphology in primates. Brain Behav Evol 84: 1930
58. Hopkins WD, Coulon O, Mangin JF (2010) Observer-independent characterization of sulcal landmarks and depth asymmetry in the central sulcus of the chimpanzee brain. Neuroscience 171:544–551
59. Cykowski MD, Coulon O, Kochunov PV, Amunts K, Lancaster JL, Laird AR et al (2008) The central sulcus: an observer-independent characterization of sulcal landmarks and depth asymmetry. Cereb Cortex 18:1999–2009
60. Bogart SL, Mangin JF, Schapiro SJ, Reamer L, Bennett AJ, Pierre PJ, Hopkins

WD (2012) Cortical sulci asymmetries in chimpanzees and macaques: a new look at an old idea. NeuroImage 61:533–541

61. Leonard CM, Towler S, Welcome S, Chiarello C (2009) Paracingulate asymmetry in anterior and midcingulate cortex: sex differences and the effect of measurement technique. Brain Struct Funct 213(6):553–569. https://doi.org/10.1007/s00429-009-0210-z
62. Paus T, Tomaiuolo F, Otaky N, MacDonald D, Petrides M, Atllas J et al (1996) Human cingulate and paracingulate sulci: attern, variabilty, asymmetry and probabilstic map. Cereb Cortex 6:207–214
63. Yucel M, Stuart GW, Maruff P, Velakoulis D, Crowe SF, Savage G, Pantelis C (2001) Hemispheric and gender-related differences in gross morphology of the anterior cingulate/paracingulate cortex in normal volunteers: an MRI morphometric study. Cereb Cortex 11:17–25
64. Amiez C, Sallet J, Hopkins WD, Meguerditchian A, Hadj-Bouziane F, Ben-Hamed S et al (2019) Sulcal organization in the medial frontal cortex reveals insights into primate brain evolution. Nat Commun 10: 3437
65. Miller EN, Hof PR, Sherwood CC, Hopkins WD (2021) The paracingulate sulcus is a unique feature of the medial frontal cortex shared by great apes and humans. Brain Behav Evol 96(1):26–36. https://doi.org/10.1159/000517293
66. Hopkins WD, Sprung-Much T, Amiez C, Procyk E, Petrides M, Schapiro SJ, Sherwood CC (2022) A comprehensive analysis of variability in the sulci that define the inferior frontal gyrus in the chimpanzee (Pan troglodytes) brain. Am J Biol Anthropol 179(1):31–47
67. Sherwood CC, Broadfield DC, Holloway RL, Gannon PJ, Hof PR (2003) Variability of Broca's area homologue in great apes: implication for language evolution. Anat Rec 217A:276–285
68. Keller SS, Deppe M, Herbin M, Gilissen E (2012) Variabilty and asymmetry of the suclal contours defining Broca's area homologue in the chimpanzee brain. J Comp Neurol 520: 1165–1180
69. Kurth F, Gaser C, Luders E (2015) A 12-step user guide for analyzing voxel-wise gray matter asymmetries in statistical parametric mapping. Nat Protoc 10(2):293–304
70. Hopkins WD, Taglialatela JP, Meguerditchian A, Nir T, Schenker NM, Sherwood CC (2008) Gray matter asymmetries in chimpanzees as revealed by voxel-based morphometry. NeuroImage 42(2): 491–497
71. Hopkins WD, Taglialatela JP, Nir T, Schenker NM, Sherwood CC (2010) A voxel-based morphometry analysis of white matter asymmetries in chimpanzees (Pan troglodytes). Brain Behav Evol 76(2):93–100
72. Keller SS, Crow TJ, Foundas AL, Amunts K, Roberts N (2009) Broca's area: nomenclature, anatomy, typology and asymmetry. Brain Lang 109:29–48
73. Keller SS, Highley JR, Garcia-Finana M, Sluming V, Rezaie R, Roberts N (2007) Sulcal variability, stereological measurement and asymmetry of Broca's area on MR images. J Anat 211:534–555
74. Schenker NM, Hopkins WD, Spocter MA, Garrison AR, Stimpson CD, Erwin JM et al (2010) Broca's area homologue in chimpanzees (Pan troglodytes): probabilistic mapping, asymmetry, and comparison to humans. Cereb Cortex 20:730–742
75. Amunts K, Schleicher A, Bürgel U, Mohlberg H, Uylings HB, Zilles K (1999) Broca's region revisited: Cytoarchitecture and intersubject variability. J Comp Neurol 412(2):319–341
76. Horwitz B, Amunts K, Bhattacharyya R, PAtkin D, Jeffries K, Zilles K, Braun AR (1999) Activation of Broca's area during the production of spoken and signed language: a combined cytoarchitectonic mapping and PET analysis. Neuropsychologia 41(14): 1868–1876
77. Paus T, Tomaiuolo F, Otaky N, MacDonald D, Petrides M, Atllas J et al (1996) Human cingulate and paracingulate sulci: pattern, variabilty, asymmetry and probabilstic map. Cereb Cortex 6:207–214
78. Tomaiuolo F, MacDonald JD, Caramanos Z, Posner G, Chiavaras M, Evans AC, Petrides M (1999) Morphology, morphometry and probability mapping of the pars opercularis of the inferior frontal gyrus: an *in vivo* MRI analysis. Eur J Neurosci 11:3033–3046
79. Hopkins WD, Taglialatela JP (2011) The role of Broca's area in socio-communicative processes in chimpanzees. In: Ferrari P, de Waal F (eds) The primate mind: built to connect with other minds. Harvard University Press, Cambridge
80. Spocter MA, Hopkins WD, Garrison AR, Stimpson CD, Erwin JM, Hof PR, Sherwood CS (2010) Wernicke's area homolog in chimpanzees (Pan troglodytes): Probabilstic mapping, asymmetry and comparison with humans. Proc R Soc B Biol Sci 277:2165–2174
81. Toga AW, Thompson M (2003) Mapping brain asymmetry. Nature 4:37–48

82. Singh M, Nagashima M, TInoue Y. (2004) Anatomical variations of ocicpital bone impressions for dural venous sinuses around the torcular Herophili, with special reference to the consideration of clinical significance. Surg Radiol Anat 26:480–487
83. Williams NA, Close JP, Giouzeli M, Crow TJ (2006) Accelerated evolution of *Protocadherin 11X/Y*: a candidate gene-pair for cerebral asymmetry and language. Am J Med Genet B (Neuropsychiatr Genet) 141B:623.33
84. Cain DP, Wada JA (1979) An anatomical asymmetry in the baboon brain. Brain Behav Evol 16:222–226
85. Holloway RL, De La Coste-Lareymondie MC (1982) Brain endocast asymmetry in pongids and hominids: some preliminary findings on the paleontology of cerebral dominance. Am J Phys Anthropol 58:101–110
86. Balzeau A, Gilissen E (2010) Endocranial shape asymmetries in *Pan panuscus, Pan troglodytes*, and *Gorilla gorilla* assessed via skull based landmark analysis. J Hum Evol 59:54–69
87. Balzeau A, Holloway RL, Grimaud-Herve D (2012) Variations and asymmetries in regional brain surface in the genus Homo. J Hum Evol 62:696–706
88. Barrick TR, Mackay CE, Prima S, Maes F, Vandermeulen D, Crow TJ, Roberts N (2005) Automatic analysis of cerebral asymmetry: an exploratory study of the relationship between torque and planum temporale asymmetry. NeuroImage 24:678–691
89. Narr KL, Bilder RM, Luders E, Thompson PM, Woods RP, Robinson D et al (2007) Asymmetries of cortical shape: effects of handedness, sex and schizophrenia. NeuroImage 34:939–948
90. Luders E, Gaser C, Jancke L, Schlaug G (2004) A voxel-based approach to gray matter asymmetries. NeuroImage 22:656–664
91. Watkins KE, Paus T, Lerch JP, Zijdenbos A, Collins DL, Neelin P et al (2001) Structural asymmetries in the human brain: a voxel-based statistical analysis of 142 MRI scans. Cereb Cortex 11:868–877
92. Phillips KA, Sherwood CS (2007) Cerebral petalias and their relationship to handedness in capuchin monkeys (Cebus apella). Neuropsychologia 45:2398–2401
93. Smith SM, Jenkinson M, Woolrich MW, Beckmann CF, Behrens TEJ, Johansen-Berg H et al (2004) Advances in functional and structural MR image analysis and implementation of FSL. NeuroImage 23(S1):208–219
94. Li X, Crow TJ, Hopkins WD, Gong Q, Roberts N (2018) Human torque is not present in chimpanzee brain. NeuroImage 165: 285–293. https://doi.org/10.1016/j.neuroimage.2017.10.017
95. Alexander AL, Lee JE, Lazar M, Field AS (2007) Diffusion tensor imaging of the brain. Neurotherapeutics 4(3):316–329
96. Basser PJ, Pierpaoli C (1996) Microstructural and physiological features of tissues elucidated by quantitative-diffusion-tensor MRI. J Magn Reson B 111:209–219
97. Rilling JK, Glasser MF, Preuss TM, Ma X, Zhang X, Zhao T et al (2008) The evolution of the arcuate fasciculus revealed with comparative DTI. Nat Neurosci 11:426–428
98. Rilling JK, Glasser MF, Jbabdi S, Andersson J, Preuss TM (2012) Continuity, divergence and the evolution of brain language pathways. Front Evol Neurosci 3(11):1–6
99. Hecht EE, Gutman DA, Bradley BA, Preuss TM, Stout D (2015) Virtual dissection and comparative connectivity of the superior longitudinal fasciculus in chimpanzees and humans. NeuroImage 108:124–137
100. Li L, Preuss TM, Rilling JK, Hopkins WD, Glasser MF, Kumar B et al (2009) Chimpanzee pre-central corticospinal system asymmetry and handedness: a diffusion magnetic reonance imaging study. PLoS One 5(9): e12886
101. Phillips KA, Schaeffer J, Barrett E, Hopkins WD (2013) Performance asymmetries in tool use are associated with corpus callosum integrity in chimpanzees (Pan troglodytes): a diffusion tensor imaging study. Behav Neurosci 127(1):106–113. https://doi.org/10.1037/a0031089
102. Iturria-Medina Y, Fernández AP, Morris DM, Canales-Rodríguez EJ, Haroon HA, Pentón LG et al (2011) Brain hemispheric structural efficiency and interconnectivity rightward asymmetry in human and nonhuman primates. Cereb Cortex 21:56–67
103. Behrens TEJ, Woolrich MW, Jenkinson M, Johansen-Berg H, Nunes RG, Clare S et al (2003) Characterization and propagation of uncertainty in diffusion-weighted MR imaging. Magn Reson Med 50(5):1077–1088
104. Behrens TEJ, Johansen-Berg H, Woolrich MW, Smith SM, Wheeler-Kingshott CAM, Boulby PA et al (2003) Non-invasive mapping of connections between human thalamus and cortex using diffusion imaging. Nat Neurosci 6(7):750–757
105. Smith SM, Jenkinson M, Johansen-Berg H, Rueckert D, Nichols TE, MacKay CE et al

(2006) Tract-based spatial statistics: voxelwise analysis of multi-subject diffusion data. NeuroImage 31:1487–1505

106. Latora V, Marchiori M (2001) Efficient behavior of small-world networks. Phys Rev Lett 87(19):198701. https://doi.org/10.1103/PhysRevLett.87.198701
107. Iturria-Medina Y (2013) Anatomical brain networks on the prediction of abnormal brain states. Brain Connect 3(1):1–21. https://doi.org/10.1089/brain.2012.0122
108. Iturria-Medina Y, Perez Fernandez A, Morris DM, Canales-Rodriguez EJ, Haroon HA, Garcia Penton L et al (2011) Brain hemispheric structural efficiency and interconnectivity rightward asymmetry in human and nonhuman primates. Cereb Cortex 21(1): 56–67. https://doi.org/10.1093/cercor/bhq058
109. Biswal BB, Yetkin FZ, Haughton VM, Hyde JS (1995) Functional connectivity in the motor cortex of resting human brain using echo-planar MRI. Magn Reson Med 34: 537–451
110. Friston KJ, Frith CD, Liddle PF, Frackowiak RSJ (1993) Functional connectivity: the principal-component analysis of large (PET) data sets. J Cereb Blood Flow Metab 13:5–14
111. Buckner RL, Vincent JL (2007) Unrest at rest: default activity and spontaneous network correlations. NeuroImage 102:1091–1096
112. Greicius MD, Krasnow B, Reiss AL, Menon V (2003) Functional connectivity in the resting brain: a network analysis of the default mode hypothesis. Proc Natl Acad Sci 100(1): 253–258
113. Lowe MJ, Dzemidzic M, Lurito JT, Mathews VP, Phillips MD (2000) Correlations in low-frequency BOLD fluctuations reflect cortico-cortical connections. NeuroImage 12(5):582–587
114. Smith SM, Fox PT, Miller KL, Glahn DC, Fox PM, Mackay CE et al (2009) Correspondence of the brain's functional architecture during activation and rest. Proc Natl Acad Sci 106(31):13040–13045
115. Hori Y, Schaeffer DJ, Gilbert KM, Hayrynen LK, Clery JC, Gati JS et al (2020) Altered resting-state functional connectivity between awake and isoflurane anesthetized marmosets. Cereb Cortex 30(11):5943–5959. https://doi.org/10.1093/cercor/bhaa168
116. Yacoub E, Grier MD, Auerbach EJ, Lagore RL, Harel N, Adriany G et al (2020) Ultra-high field (10.5 T) resting state fMRI in the macaque. NeuroImage 223:117349. https://doi.org/10.1016/j.neuroimage.2020.117349
117. Vincent JL, Patel GH, Fox MD, Synder AZ, Baker JT, Van Essen DC et al (2007) Intrinsic functional architecture in the anaesthetized monkey brain. Nature 447:83–86
118. Hutchison RM, Leung LS, Mirsaattari SM, Gati JS, Menon RS, Everling S (2011) Resting-state networks in the macaque at 7T. NeuroImage 56:1546–1555
119. Beckmann CF, DeLuca M, Devlin JT, Smith SM (2005) Investigations into resting-state connectivity using independent components analysis. Philos Trans R Soc Lond B Biol Sci 360:1001–1013
120. Damoiseaux JS, Rombouts SARB, Barkhof F, Scheltens P, Stam CJ, Smith SM, Beckmann CF (2006) Consistent resting-state networks across healthy subjects. Proc Natl Acad Sci 103(37):13848–13853
121. Sengupta A, Wang F, Mishra A, Reed JL, Chen LM, Gore JC (2023) Detection and characterization of resting state functional networks in squirrel monkey brain. Cereb Cortex Commun 4(3):tgad018. https://doi.org/10.1093/texcom/tgad018
122. Belcher AM, Yen CC, Stepp H, Gu H, Lu H, Yang Y et al (2013) Large-scale networks in the awake, truly resting marmoset monkey. J Neurosci 33:16796–16804
123. Liu JV, Hirano Y, Nascimento GC, Stefanovic B, Leopold DA, Silva AC (2013) fMRI in the awake marmoset: somatosensory-evoked responses, functional connectivity, and comparison with propofol anesthesia. NeuroImage 78:186–195. https://doi.org/10.1016/j.neuroimage.2013.03.038
124. Wey HY, Phillips KA, McKay DR, Laird AR, Kochunov P, Davis MD et al (2014) Multi-region hemispheric specialization differentiates human from nonhuman primate brain function. Brain Struct Funct 219(6): 2187–2194. https://doi.org/10.1007/s00429-013-0620-9
125. Belcher AM, Yen CC, Stepp H, Gu H, Lu H, Yang Y et al (2013) Large-scale brain networks in the awake, truly resting marmoset monkey. J Neurosci 33(42):16796–16804. https://doi.org/10.1523/JNEUROSCI.3146-13.2013
126. Silva AC, Liu JV, Hirano Y, Leoni RF, Merkle H, Mackel JB et al (2011) Longitudinal functional magnetic resonance imaging in animal models. Methods Mol Biol 711:281–302. https://doi.org/10.1007/978-1-61737-992-5_14

127. Lopez-Persem A, Roumazeilles L, Folloni D, Marche K, Fouragnan EF, Khalighinejad N et al (2020) Differential functional connectivity underlying asymmetric reward-related activity in human and nonhuman primates. Proc Natl Acad Sci USA 117(45): 28452–28462. https://doi.org/10.1073/pnas.2000759117
128. Howells H, Simone L, Borra E, Fornia L, Cerri G, Luppino G (2020) Reproducing macaque lateral grasping and oculomotor networks using resting state functional connectivity and diffusion tractography. Brain Struct Funct 225(8):2533–2551. https://doi.org/10.1007/s00429-020-02142-2
129. Murphy K, Birn RM, Bandettini PA (2013) Resting-state fMRI confounds and cleanup. NeuroImage 80:349–359
130. Teichert T, Grinband J, Hirsch J, Ferrera VP (2010) Effects of heartbeat and respiration on macaque fMRI: implications for functional connectivity. Neuropsychologia 48:1886–1894
131. Goense JB, Whittingstall K, Logothetis NK (2010) Functional magnetic resonance imaging of awake behaving macaques. Methods 50:178–188
132. Andersen AH, Zhang Z, Barber T, Rayens WS, Zhang J, Grondin R et al (2002) Functional MRI studies in awake rhesus monkeys: methodological and analytical strategies. Methods 118:141–152
133. Logothetis NK, Guggenberger H, Peled S, Pauls J (1999) Functional imaging of the monkey brain. Nat Neurosci 2:555–562
134. Hutchison RM, Everling S (2014) Broad intrinsic functional connectivity boundaries of the macaque prefrontal cortex. NeuroImage 88:202–211. https://doi.org/10.1016/j.neuroimage.2013.11.024
135. Vincent JL, Patel GH, Fox MD, Snyder AZ, Baker JT, Van Essen DC et al (2007) Intrinsic functional architecture in the anaesthetized monkey brain. Nature 447(7140):83–86. https://doi.org/10.1038/nature05758
136. Margulies DS, Bottger J, Long X, Lv Y, Kelly C, Schafer A et al (2010) Resting developments: a review of fMRI post-processing methodologies for spontaneous brain activity. MAGMA 23:289–307
137. Hutchison RW, Everling S (2012) Monkey in the middle: why non-human primates are needed to bridge the gap in resting-state investigations. Front Neuroanat 6:20
138. Rilling JK, Barks SK, Parr LA, Preuss TM, Faber TL, Pagnoni G et al (2007) A comparison of resting-state brain activity in humans and chimpanzees. Proc Natl Acad Sci 104(43):17146–17151
139. Kojima T, Onoe H, Hikosaka K, Tsutsui KI, Tsukada H, Watanabe M (2009) Default mode of brain activity demonstrated by positron emission tomography imaging in awake monkeys: higher rest-related than working memory-related activity in medial cortical areas. J Neurosci 29(46):14463–14471. https://doi.org/10.1523/JNEUROSCI.1786-09.2009
140. Barks SK, Parr LA, Rilling JK (2015) The default mode network in chimpanzees (Pan troglodytes) is similar to that of humans. Cereb Cortex 25:538–544
141. Parr LA, Hecht E, Barks SK, Preuss TM, Votaw JR (2009) Face processing in the chimpanzee brain. Curr Biol 19:50–53
142. Taglialatela JP, Russell JL, Schaeffer JA, Hopkins WD (2008) Communicative signaling activates "Broca's" homolog in chimpanzees. Curr Biol 18:343–348
143. Taglialatela JP, Russell JL, Schaeffer JA, Hopkins WD (2009) Visualizing vocal perception in the chimpanzee brain. Cereb Cortex 19(5): 1151–1157
144. Gil-da-Costa R, Martin A, Lopes MA, Munoz M, Fritz JB, Braun AR (2006) Species-specific calls activate homologs of Broca's and Wernicke's areas in the macaque. Nat Neurosci 9(8):1064–1070
145. Poremba A, Malloy M, Saunders RC, Carson RE, Herscovitch P, Mishkin M (2004) Species-specific calls evoke asymmetric activity in the monkey's temporal poles. Nature 427:448–451
146. Hopkins WD (2022) Neuroanatomical asymmetries in nonhuman primates in the homologs to Broca's and Wernicke's areas: a mini-review. Emerg Top Life Sci. https://doi.org/10.1042/ETLS20210279

Chapter 17

Imaging Techniques in Insects

Marco Paoli, Mara Andrione, and Albrecht Haase

Abstract

The present chapter describes how to investigate brain lateralization in insects with methods of optical neuroimaging. It provides two complete protocols, one for in vivo imaging to obtain information on functional lateralization, and one for histochemical techniques to study morphological asymmetries. Both sections start with the animal preparation, illustrate the different possibilities for brain tissue labeling, and review the available imaging techniques, concentrating on widefield fluorescence microscopy, confocal, and two-photon laser scanning microscopy. After some remarks on the main methods for data analysis, studies on functional and morphological lateralization in insects are reviewed.

Key words Lateralization, Calcium Imaging, Two-photon microscopy, Honeybee, *Drosophila*

1 Introduction

The discovery of brain lateralization in insects [1, 2] opened up a promising new test ground for one of the most exciting questions in evolutionary neuroscience: the origin of brain asymmetry [3–5]. While the first results were reported from behavioral studies (for a review, *see* [6]), subsequently, attention focused also on the underlying mechanisms within the insect brain. Initially, brain functions were mainly studied using electrophysiology [7, 8], which offered the most direct access to neuronal activity. However, although the strength of this method is the direct measurement of local activity, it does not allow detecting precise response pattern distribution. Therefore, scientists started to develop functional imaging of insect brains, which succeeded in the early 1990s [9] and became a standard tool shortly after [10, 11]. Initial studies on functional lateralization, whose sensitivity and resolution were still relatively low, were unable to reveal significant effects [12]. With the recent advances in 3D in vivo imaging technology and molecular biology, functional imaging has overcome these limitations. Today, optical imaging represents a promising method to study both morphological and functional lateralization [13]. This chapter

Lesley J. Rogers and Giorgio Vallortigara (eds.), *Lateralized Brain Functions: Methods in Human and Non-Human Species*, Neuromethods, vol. 217, https://doi.org/10.1007/978-1-0716-4240-5_17,

aims to provide a guideline through the multitude of available methods of sample preparation, image acquisition, and data post-processing. We have concentrated on their implementation to investigate lateralization in the honeybee *Apis mellifera* and the fruit fly *Drosophila melanogaster*, but most of the techniques can be easily adapted to study other insect species.

2 In Vivo Imaging

The antennal lobe (AL) is the primary olfactory center of the insect brain and the functional equivalent of the vertebrate olfactory bulb [14]. Due to its primary role in sensory coding and perception, and its favorable position in terms of optical accessibility, the AL represents one of the most common anatomical models to investigate functional brain lateralization in invertebrates. Antennal lobe in vivo imaging can be performed using a similar protocol in different insect species. In both honeybees and fruit flies, olfactory information is conveyed via olfactory receptor neurons (ORNs) to the AL, with ORNs of the same receptor family (i.e., expressing the same odor receptor protein) converging onto a single glomerulus, the AL anatomical and functional unit. The honeybee AL consists of about 160 roughly spherical glomeruli of diameter $d \approx 50$ μm [15], while the fruit fly AL consists of about 54 glomeruli of $d \approx 20$ μm [16]. Glomeruli are densely packed into a bi-dimensional layer to form the shell of the antennal lobe, which reaches an overall $d \approx 400$ μm in the honeybee, and $d \approx 80$ μm in the fruit fly. Local neurons (LNs) synapse among glomeruli within each AL, and from each glomerulus, projection neurons (PNs) relay the processed olfactory signal to central brain areas, such as the mushroom bodies (MBs) and the lateral horn (LH) (Fig. 1).

2.1 Preparation

2.1.1 Honeybee

To obtain fluorescently stained antennal lobes for calcium imaging analysis in the honeybee, two main approaches might be followed. The first one consists of staining all cell types present in the AL and measuring the overall activity. The second one aims to measure the activity of a selected cellular population, the AL projection neurons. In the first case, a cell-permeable calcium sensor is applied as bath staining onto the brain. With the second approach, a membrane-impermeable calcium indicator is injected into the antennal lobe tracts, where it will be absorbed by the projection neurons' axonal branches. Within ~6 h, the dye will diffuse retrogradely to the PNs' cell bodies and dendrites. The advantage of selective probe-injection is the specificity of the fluorescent signal collected, and the higher contrast. Disadvantages are the long preparation time and the lower success rate. Notably, the protocol described in the following paragraph was established in the honeybee but has been successfully transferred to other insect models, such as the

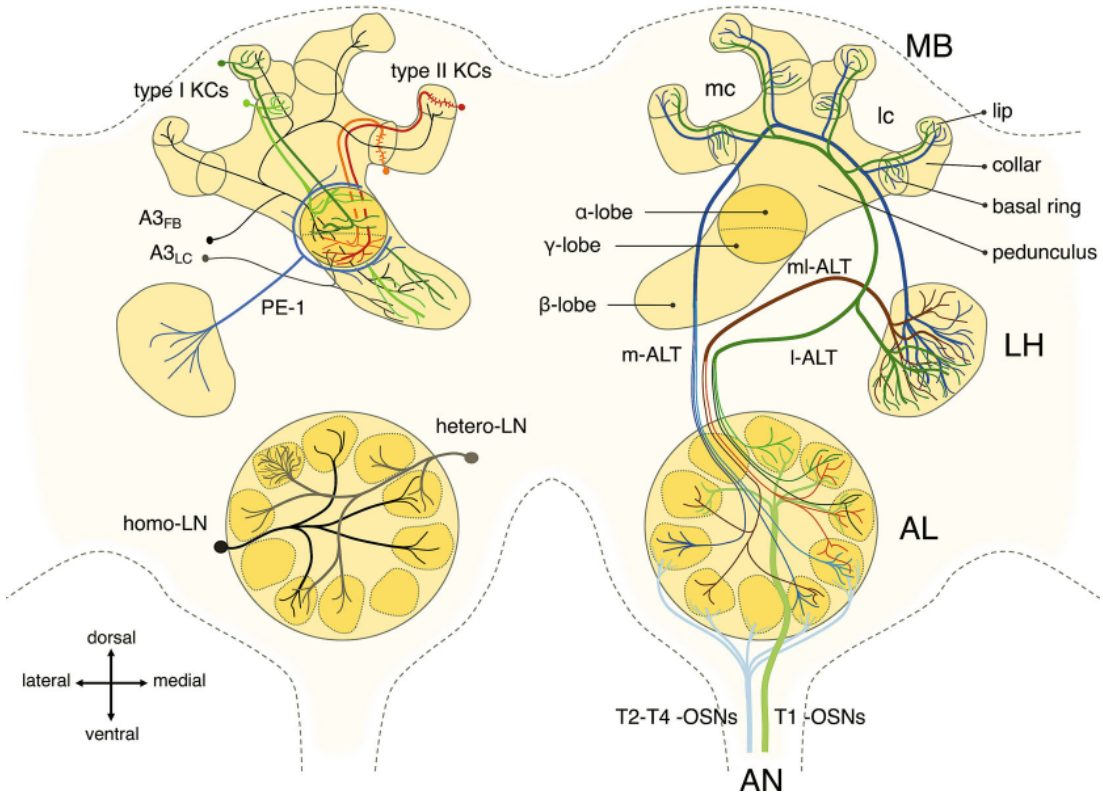

Fig. 1 The honey bee olfactory circuit. For clarity, different neuron types and neuronal tracts are labelled with different colours and presented in different hemispheres. Four antennal nerve (AN) tracts (T1 to T4) comprising the axons of ~60,000 olfactory sensory neurons (OSNs) innervate the antennal lobe (AL). All OSNs bearing the same olfactory receptor converge onto one of ~165 glomeruli, the structural and functional units of the AL. The convergent input is processed by a local network of ~4000 local interneurons (homo- and hetero-LNs). Then, the information is relayed to higher-order processing centers—the mushroom body (MB) and the lateral horn (LH) by ~800 AL projection neurons (PNs) via the medial and lateral antennal lobe tracts (m- and l-ALT). Olfactory PNs innervate the lip and the basal ring of the MB calyces—whereas the collar region is dedicated to the processing of visual input—and synapse onto the MB intrinsic neurons, the Kenyon cells (KCs). KCs' axons descend in parallel fibers from the MB calyces, and they bifurcate to innervate the MB lobes. (Reprinted from [14] with kind permission from Springer Science+Business Media)

American cockroach *Periplaneta americana* [17] and the locust *Schistocerca gregaria* [18].

These methods described here consist of adaptations of the procedures developed in the late 1990s by Galizia and collaborators [12]. Briefly, bees are collected upon arrival at a feeder to which they were previously familiarized. This allows the selection of forager bees, which are usually preferred over younger/male bees for olfaction studies. Collected bees can be labeled right away or transferred into small plastic cages, fed, and placed in an incubator at 30 °C until the next day. Immediately before starting the staining procedure, the bees are transferred from the box into small plastic tubes with perforated lids.

To cold-anesthetize the bee, the plastic tube is placed on ice for 3–4 min until the bee stops moving (note that excessive permanence of the bee at low temperatures markedly affects the bee's survival). Once the bee has been immobilized, it is mounted onto a custom-made plexiglass structure by gently sliding its neck through a thin stage fissure (Fig. 2). This operation is carried out with large rounded-end entomological forceps to prevent the bee from being damaged. Immediately after, a small rectangular piece of plastic foil (≈7 × 4 mm) is placed onto the stage behind the bee's head, thereby applying a slight pressure to push the neck forward. The foil is attached to the mounting stage with hard wax (e.g., Siladent, Deiberit 502) or bee wax melted with the hot tip of a soldering iron (80 °C). It is important to avoid touching the bee's antennae with the hot wax, as the temperature may damage the olfactory sensory neurons. To further limit head movements, the head can be surrounded by soft dental wax (e.g., Kerr, Soft Boxing Wax Sticks). This kind of wax becomes malleable when warmed by hand, and it can be handled comfortably using a wooden toothpick and spread all around the bee head to hold it in position.

The next step consists of opening the head cuticle and exposing the brain. To preserve the antennae from damage, they can be blocked in a forward-facing position by insect pins or by placing a small drop of eicosane (Sigma-Aldrich, CAS 112-95-8) at the bases of the antennae while holding them frontally with a toothpick. Eicosane is a low melting temperature (40 °C) hydrocarbon that hardens within 2–3 s, allowing to hold the antennae in position during the labeling procedure. The cuticle is then incised with a scalpel to open a window bordered by the antenna sockets on its anterior side, by the ocelli on its posterior side, and by one of the compound eyes on the lateral side. On the side without a cut, a third insect pin is placed into the wax to act as a vertical fulcrum and keep the cuticle window open. Afterward, glands and tracheae covering the neural tissue are pushed aside or removed with precision forceps to reveal the whole area of interest: the antennal lobe, in the case of bath staining, or the injection point (i.e., the

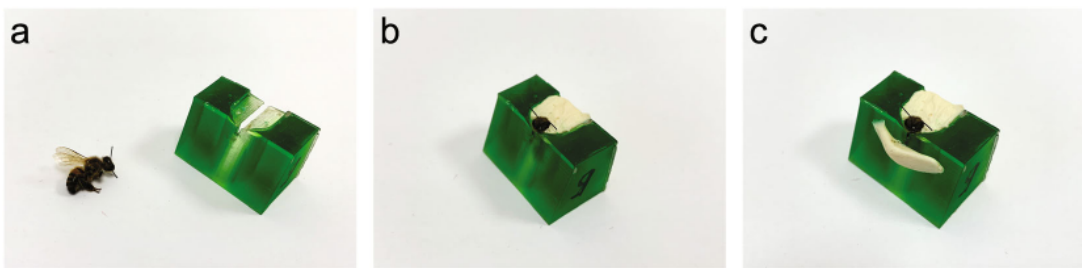

Fig. 2 Animal preparation using a plexiglass mounting stage (**a**). After sliding the bee's neck into the thin stage fissure (**b**, **c**), the head is blocked with a thin plastic foil, and sealed to the mounting stage with hard wax. The head can be further immobilized with soft dental wax

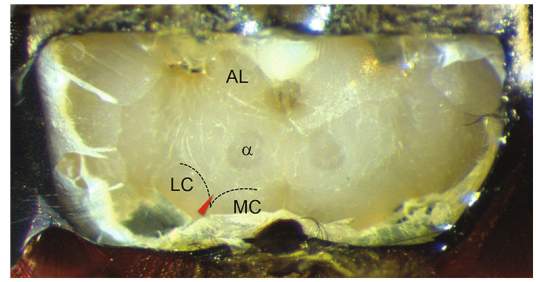

Fig. 3 Backfilling of antennal lobe projection neurons. The dye is injected at the intersection between the lateral and medial antennal lobe tracts (red arrowhead). The site can be recognized as a small indent between the medial (MC) and lateral calyces (LC) of the mushroom bodies, which border the posterior part of the brain. The α-lobe (α) may also be used as a reference

intersection between the lateral and medial antennal lobe tracts (l- and m-ALT); Fig. 3) in the case of PNs' backfilling.

In the case of bath staining, the brain is incubated for about 1 h with a drop of dye dissolved at the appropriate concentration. During this time, the cuticle window should be closed and sealed with eicosane in order to prevent the brain from drying. For PN backfilling, dye injection is performed with a tapered glass capillary, previously pulled to a tip size of a few micrometres. For loading the capillary, dry dye crystals should be placed on a clean glass slide and dissolved into a highly viscous solution with a minimal amount of distilled water (<1 μl). When the solution's viscosity allows it, the capillary can be used as a spoon to collect a small blob of dye. The loaded tip is then inserted into the tissue between the mushroom body calyces (Fig. 3) [19] and kept in place until the dye dissolves. After the injection, the cuticle window is closed and sealed with liquid eicosane, the antennae are freed, and the bee is fed on a 50% sucrose solution and kept in the dark at room temperature.

On the following day (or one hour after in case of bath staining incubation), labeled bees are prepared for imaging in a manner that allows clear optical access to the brain and suppresses all possible movements. This becomes even more critical when working with laser scanning microscopes since a displacement of a few micrometers in any direction will cause large artifacts. Once again, the antennae are gently placed in a forward-facing position and the cuticle window is re-opened to expose the antennal lobe. A piece of plastic foil matching the shape of the mount and the bee's head is placed between the antennae and cuticle window and fixed with melted hard wax to the plexiglass mount to isolate the antennae from the imaging area. Finally, the regions around the cuticle window are sealed with a bi-component silicone elastomer (Kwik-Sil, WPI) to form a water-proof environment for the physiological solution (Ringer solution: 130 mM NaCl, 6 mM KCl, 4 mM $MgCl_2$, 5 mM $CaCl_2$, 160 mM sucrose, 25 mM glucose, 10 mM

HEPES, pH 6.7, 500 mOsmol [20]). Alternatively, the whole brain can be covered in transparent Kwik-Sil. This has the advantage of a more stable brain preparation and avoids introducing excessive fluid in the animal's head. On the other hand, this method is not suitable for pharmacological experiments since access to the brain for drug administration is blocked by the silicon. As a last step, a piece of foam gently pressed against the bee's thorax and abdomen can further reduce body movements, which may cause motions within the head.

2.1.2 Fruit Fly

The preparation of *Drosophila melanogaster* for in vivo functional imaging is particularly delicate due to its small size. Bearing this in mind, the preparation in itself closely resembles the protocol adopted for honeybee handling described above.

For optimal preparation, flies of an age between 4 and 15 days old are preferred. At a younger age, the head cuticle is still very soft, and it is difficult to perform precise cuts. In addition, females are bigger, and, therefore, easier to manipulate. Before handling, flies are briefly immobilized (<1 min) in an ice-cooled petri dish. While anesthetized, they are placed onto a custom-made plexiglass mount, where a thin copper plate, cut in the middle, had been previously installed. The fly is slid by its neck through the slit across the copper plate, where the head is held in place by a small drop of colophony resin applied between the eyes and the copper plate. In this way, the head of the fruit fly is still, while the body and legs are free to move. At this stage, the antennal plate is carefully pulled forward with surgical forceps, and a thin metal wire (0.015-mm thick) is gently inserted along the frontal suture to keep the antennae in a forward-facing position, and the antennal plate slightly detached from the head. A small piece of polyethylene foil, with a $\approx$ 0.5 mm wide square hole in the middle, is placed above the head in such a way that eyes and antennae are covered by the foil, but the head cuticle behind the antennae remains accessible. At this point, a thin layer of two-component silicone (Kwik-Sil, WPI) is used to seal the fissures between the polyethylene foil and the head to prevent the preparation from leaking. Using a sharp sapphire blade, a window is cut through the cuticle to expose the brain, which must be rapidly covered with a drop of Ringer solution [20]. Finally, tracheae and glands obstructing the view can be removed [21, 22].

A successful operation will be characterized by a very lively animal, whose legs will be actively moving during the experimental session. This may produce small movements of the fly's brain during image acquisition. Compared to the honeybee, the fruit fly is more delicate and less resistant to the described manipulation or long imaging sessions. This drawback is compensated by the advantages of working with an animal model for which a wide array of genetic tools is available.

2.2 Functional Indicators

In vivo imaging in the honeybee and in *Drosophila* allows the investigation of neural activity. In the following sections, we will introduce organic dyes and genetically encoded indicators that are most relevant for functional imaging analysis and suitable for studying neural dynamics and lateralization in the olfactory circuit.

2.2.1 Organic Dyes

Voltage-sensitive dyes (VSDs) are membrane-binding chromophores that quickly modify their absorption/emission fluorescence intensity in response to modulation of the membrane potential. Hence, optical imaging using VSDs represents a direct measure of neuronal activity, allowing insights into fast cellular dynamics (e.g., action potentials and sub-threshold potentials). Like other optical methods, it allows the following of a large subset of neurons or even an entire brain simultaneously. The main limitation of this approach is the low signal-to-noise ratio [23]. Nongenetically encoded VSDs are delivered via bath application. Bath-applied dyes will interact nonspecifically with any cell membrane in the preparation so that various sources of fluorescence fluctuations may mask the relevant signals. Furthermore, even reducing the nonspecific signal by intracellular delivery of the functional reporter, the relatively low amount of membrane available for the dye to interact with, compared to the total cellular volume available, greatly limits the detectability of the fluorescence changes with respect to cytoplasmic calcium sensors [24].

For these reasons, VSD-based methodology has not been broadly applied yet. Relevant publications include two studies from Galizia and collaborators [25, 26], who used the voltage-sensitive dye RH795 (excitation/emission wavelengths of 530/712 nm) to investigate honeybee olfactory coding. For those experiments, it was necessary to average over 8 to 16 odor stimulation responses in order to reach an acceptable signal-to-noise ratio. The dye helped reveal important insights into the phasic-tonic behavior of different glomeruli in response to different odorants. Anyhow, because of the staining approach adopted in that study, it was not possible to disentangle the contributions of different cell types (PNs, ORNs, and LNs) to the detected signals.

The gold standard in functional insect brain imaging is calcium-sensitive dyes. This approach relies on fluorescent probes, which were derived from the structures of calcium chelators such as ethylene glycol tetraacetic acid (EGTA) and bis(2-aminophenoxy)ethane-N,N,N′,N′-tetraacetic acid (BAPTA) [27] and modulate their excitation/emission spectra when interacting with calcium. Thus, via fluorescence microscopy, it is possible to relate changes in fluorescence to changes in intracellular calcium concentration. This provides a reliable proxy of neuronal activity [28] and a widely accepted technique for the investigation of neurophysiology [29, 30]. Some calcium-sensitive dyes—ratiometric dyes—allow absolute measurements of intracellular calcium concentration with

high accuracy by exploiting the properties of their absorbance spectrum. Ratiometric calcium imaging requires two measurements taken in rapid sequence: The first one at the excitation wavelength showing the maximum ratio between the fluorescence intensity of calcium-bound and calcium-free states (e.g., 340 nm in Fura-2), the second one at the excitation wavelength showing a minimum ratio between the two values (e.g., 380 nm in Fura-2). The emitted fluorescence is measured in both cases at the maximum of the emission peak (510 nm in Fura-2). The ratio between the two measured values ($F_{340\ \mathrm{nm}}/F_{380\ \mathrm{nm}}$) is an estimate of the absolute calcium concentration, independently of artifacts due to uneven dye distribution among the cells. This sequential imaging technique is well suited for widefield microscopy, whereas laser-scanning techniques do not allow alteration of the excitation wavelength with the required speed [28].

The first calcium imaging data on olfactory coding were collected using the bath-staining approach. The dyes of choice for these preparations were cell-permeable acetoxymethyl (AM) ester forms Calcium Green-1 and Calcium Green-2. The AM coating makes the dyes electrically neutral, allowing them to cross the lipid bilayer of the cell membrane. Once inside the cell, the AM groups are removed by endogenous esterases, trapping the chromophore (now electrically charged) inside the cytoplasm.

The introduction of the PNs backfilling method [19] allowed, for the first time, to obtain a signal originating from a defined cellular population (*see* Subheading 2.1.1). Although the signals obtained through the two approaches are correlated [19], it is preferable to adopt neuronal backfilling over bath staining since the collection of cell-specific calcium signals makes it easier to draw relevant conclusions about the network's properties. Nowadays, most functional imaging studies conducted in the honeybee brain are performed using the Fura-2 fluorescent reporter, and cell population specificity is obtained through selective PN staining. The ratiometric properties of the dye are exploited in the case of single-photon excitation by sequential excitation at 340/380 nm. Instead, in two-photon microscopy, a single excitation wavelength at ≈780 nm is used (*see* Table 1).

2.2.2 Genetically Encoded Indicators

A drawback of the use of organic calcium-sensitive dyes is the invasiveness of the technique. The use of genetically modified model organisms allows circumventing this problem via in situ expression of genetically encoded functional indicators [31, 32]. During the last two decades, genetically encoded fluorescent reporters have been developed and applied to different animal models to track different aspects of neuronal activity, i.e., intracellular calcium concentration [33, 34], membrane potential [35, 36], synaptic vesicle cycling [37], or chloride concentration [38, 39].

Table 1
Most common probes in fluorescent imaging. In the grey sections are reported the most common calcium-sensitive probes. The maximum single-photon and two-photon excitation wavelength, the emission wavelengths [116–119]

Fluorescent probe	Single-photon Excitation wavelength [nm]	Two-photon Excitation wavelength [nm]	Dichroic cut-off wavelength [nm]	Emission wavelength [nm]
Alexa350	343	690	415	441
Hoechst33258	352	690	415	455
DAPI	358	690	415	463
Lucifer yellow	428	–	470	536
GFP	488	900–1000	495	507
RH795	490	1040	580	688
Alexa488	490	985	495	525
FITC	490	947	495	525
Rhodamin-123	507	913	515	529
Cy-3	552	1032	565	570
Alexa 546	556	1028	565	573
Alexa555	553	–	565	568
TRITC	557	–	565	576
Alexa594	590	1040	600	617
Alexa647	650	–	660	665
cal520	493	–	495	515
fura-2	360* (340**)	780	416	510
indo-1	338	700	444	475* (400**)
fluo-3	506	810	514	526
fluo-4	494	810	505	516
Calcium Green-1	507	820	514	529
GCaMP-6	488	940	495	512

*calcium-free, **calcium-bound, and an appropriate cut-off wavelength for the dichroic filter to separate emission from excitation light are given (data from Chroma Technology and Thermo Fisher Scientific)

The first generation of genetically encoded calcium indicators (GECI) relies on a Förster resonance energy transfer (FRET) effect between two green fluorescent protein (GFP) variants, one acting as an electron-donor, the other as an electron acceptor, linked together by a calcium-binding module based on the binding domain of calmodulin. In the presence of calcium, the two

fluorescent proteins undergo conformational changes reducing their intermolecular distance, and energy transfer from the donor to the acceptor protein takes place. If the donor chromophore is continuously excited, an increase in intracellular calcium can be detected by a decrease in emission intensity from the donor and an increase in emission intensity from the acceptor molecule. This is true in the case of Cameleon-like calcium indicators [33]. A second generation of calcium sensors was developed based on a single GFP-like protein coupled to a calcium-binding domain. This is the case of the widely used GCaMP indicators [34]. In GCaMPs, a GFP protein has been circularized, and new C- and N-terminals have been introduced and linked to a calmodulin sequence and a calmodulin-binding peptide. The interaction with calcium ions induces a conformational change in the protein, which enhances its fluorescence emission. Both types of chromophores have been refined over the years to improve various parameters (e.g., sensibility, dynamic range, and brightness), and they have been used extensively to study the neuronal activity within the mammalian and insect brain [40, 41].

A more direct way of monitoring neuronal activity is to measure changes in membrane potential via genetically encoded voltage indicators (GEVIs). However, the short duration of voltage changes demands faster kinetics and higher sensitivity for imaging, physical constraints that have hindered the development of GEVIs. Moreover, voltage biosensors are necessarily associated with the plasma membrane, strongly reducing the active imaging volume and worsening the signal-to-noise ratio. A first generation of voltage dyes was generated by coupling a fluorescent reporter to a voltage-gated ion-channel protein (i.e., FlaSh [35], SPARC [42]), or to its voltage-sensitive domain (VSFP 1 [36]). Later, other indicators were developed based on the voltage-sensitive domain of a phosphatase of *Ciona intestinalis* (Ci-VSP [43]), including VSFP2.3 and VSFP butterfly 1.2, both successfully expressed in the mouse cortex and used to monitor neuronal activity in vivo [32].

In conclusion, GEVIs' main advantage is to provide a direct coverage of neuronal activity, including sub-threshold potential variations. On the other hand, GECIs show slower kinetics but a wider dynamic range and are better suited for detecting large calcium transients following action potentials. Therefore, both sensors can be used to capture complementary aspects of neuronal dynamics.

2.2.3 Transgenic Insect Lines

The first genetically encoded functional indicators were expressed in the fruit fly *Drosophila melanogaster* [44]. GCaMP, the current gold standard, was first expressed in flies in 2003 [45]. Since then, all further improvements up until the last version, jGCaMP8, are

first tested in flies [46]. Also, the first expression of a voltage indicator within an intact organism was conducted in *Drosophila* [47], allowing to detect both subthreshold events and action potentials in individual cells and neuronal populations.

For a significant period, fruit flies were the only insects in which genetically encoded indicators could be employed. However, the introduction of the PiggyBac transposon system [48] and of the CRISPR/Cas9 technology [49] opened up the possibility of applying this technique to other insect models. Driven by the worldwide epidemiological burdens, scientists became increasingly interested in the mosquito *Aedes aegypti*, the primary vector for dengue, yellow fever, and Zika. Using the CRISPR/Cas9 technology they obtained genetically-modified mosquitoes expressing the GCaMP6s calcium indicator [50]. More recently, mosquito lines with pan-neuronal expression of GCaMP have been made available [51], and detailed protocols for two-photon imaging have been published [52].

The development of genetically modified honeybees is hindered by their complex reproductive biology. First, only the queen could be targeted for the creation of transgenic lines, and each genetically modified queen had to be reared in a separate colony. Then, bee rearing cannot be achieved indoors, but it requires large outdoor cages, from which transgenic bees cannot escape into nature. This was finally achieved in 2014 when Schulte et al. reported on the integration and expression of piggyBac-derived cassettes in the bee genome [53]. Based on this method, Carcaud and colleagues created the first transgenic beeline expressing GCaMP6f under the control of the synapsin promoter [54].

Recently, a piggyBac-based protocol was developed to express GCaMP6s in clonal raider ants [55]. The expression was driven by the olfactory receptor co-receptor (Orco) promoter to express the marker in olfactory sensory neurons and investigate the neural correlates of different ant alarm pheromones.

2.3 Stimulus Generator

The analysis of functional lateralization in the olfactory system requires a well-designed olfactory stimulator, which needs (1) to produce a stimulus of a consistent intensity across time and trials, (2) to ensure a fast stimulus onset and offset, and (3) to avoid biases in the geometric properties of the resulting airflow, which could transmit lateralized information to the animal.

In the past, olfactory research relied on commercially available setups such as the Stimulus Air Controller CS-55 (Syntech). Nowadays, less expensive and more reliable olfactory stimulators can be custom-built. An effective apparatus was developed by Szyszka and colleagues [56] and later replicated in the research group of A. Haase. In these devices, the switch between background airflow and olfactory stimulus is tightly controlled by high-precision solenoid valves (Lee Products Ltd.), providing a temporal millisecond

resolution of the stimulus onset/offset. Stimulus reproducibility was enhanced by loading odor fragrances in Teflon-sealed glass vials. This expedient prevents evaporation and helps to maintain the stimulus intensity constant across experimental sessions. However, a characterization of the odor signals should be performed at regular intervals using a photoionization detector to ensure stimulus reproducibility. Finally, these devices comprise multiple odor channels that can be independently controlled via computer and combined together to investigate the neural activity elicited by multiple odorants or by odor mixtures [57].

Recently, Raiser and colleagues ameliorated their previous olfactory stimulator [56] featuring a more precise control of the stimulus dynamics [58]. The improved setup can produce odorant fluctuations up to 70 Hz for two odorant channels simultaneously, thus allowing the generation of arbitrary mixtures of independently fluctuating components. The device is reliable and reproducible, making it easy to replicate the experimental setup across labs [59, 60].

If the aim is to collect the odor responses triggered by a large number of samples and concentrations, an alternative option is to use a computer-controlled autosampler, such as the commercially available PAL System (CTC Analytics AG). This system is built for high-throughput data collection and can automatically sample tens of odors in sequence [17, 61]. Via a syringe, the PAL System collects the selected volume of headspace from a sealed glass vial and injects it into a constant flow of clear air with the programmed injection speed. After each injection, the syringe is rinsed with nitrogen and washed with pentane to minimize the presence of residual odorant between subsequent measurements. Finally, a dedicated software allows easy manipulation of injection parameters (e.g., injected volume, injection time, number of pulses, and injection speed), as well as the number of analyzed samples, and intensity of the syringe cleaning procedure [61].

2.4 Image Acquisition

Nowadays, insect brain imaging is almost entirely based on fluorescence microscopy. Fluorescent indicators are excited at a specific wavelength, and the emitted fluorescence signal is collected at their peak emission wavelength. The basic hardware required for this procedure is a light source, microscope optics (e.g., filters and objectives), and a detector (i.e., camera, photomultiplier, or avalanche photodiode). Which types of each of these components are required depends on the imaging modality of choice as well as on the available budget. In the following sections, we will describe the different options available, together with their advantages and disadvantages.

2.4.1 Widefield Microscopy

Widefield microscopy is the classical implementation of fluorescence microscopy, where the whole field of view is excited at once via a wide field light source, and spatial information is obtained by detecting the fluorescence light through a 2D array of detectors.

Pros and Cons

The advantages of this approach are contained costs, simplicity, and robustness. Its limitations arise because fluorescence excitation is not confined to a single focal plane, causing signal contributions from off-focus excited regions to reduce axial resolution. Moreover, the off-focus excitation causes a large sample volume to absorb light continuously, which enhances both photo-damage and photo-bleaching effects. Finally, most fluorescent markers are excited by blue or green light. These wavelengths are strongly scattered within the tissue, thus limiting the imaging depth.

Light Sources

Typical light sources in widefield fluorescence imaging are broadband gas discharge lamps. The most common ones are mercury vapor lamps or xenon arc lamps. Their working principle is very similar, except for dimensions and enclosed gases. Mercury lamps produce, on top of a continuous spectrum, several characteristic peaks around wavelengths of 365, 400, 440, 546, and 580 nm. Xenon lamps have a more uniform intensity profile across the entire visible spectrum. Therefore, the choice of the light source should be guided by the fluorescent probe: If the excitation bands of the markers overlap with the mercury lines, a mercury lamp might be the better choice; otherwise, the uniformly distributed spectrum of the xenon lamp represents a more universal solution. The authors use a 120 W mercury-vapor lamp with a lifespan of 2000 h (X-Cite 120Q).

Optics

The optics are based on a standard epifluorescence microscope, meaning that the sample is illuminated from above, and the signal is collected through the same objective in the opposite direction. This optical conformation requires the separation of the induced fluorescent signal from the backscattered excitation light. This can be achieved with the introduction of dichroic mirrors and additional blocking filters in the detection arm. The necessary filters comprise (1) an excitation filter along the illumination pathway that limits the bandwidth of the white light source to the excitation window of the dye, (2) a dichroic mirror that separates the elicited fluorescence from the excitation light, and (3) an emission filter along the detection pathway, which additionally blocks all the light outside of the marker's emission window. Filter combinations for the most frequently used dyes can be found in Table 1.

The main optical component is the objective. To choose the correct objective, one should know beforehand:

- What magnification is required for the planned experiments?
- What is the field of view that needs to be covered?

- If any immersion liquid will be used (i.e., water and oil).
- In which spectral range (excitation/emission) the analysis will be performed.

Apart from these parameters, an optimal objective should offer the highest possible numerical aperture since this guarantees the highest possible light-collection angle and the best resolution.

Finally, the signal must be split between the ocular lenses, needed for live observation, and the detector, which is required for image recording. This is commonly achieved with a switchable mirror. Semi-transparent mirrors or transparent camera chips are also available, but both cause partial signal loss during data acquisition.

Detectors

Since widefield microscopy is a scanless technique, spatial resolution is created by the detector. The most common detectors are CCD (Charge-Coupled Device) and CMOS (Complementary Metal Oxide Silicon) cameras. While CCD technology is more mature, acquisition speed and low costs mostly favor CMOS cameras. When choosing the best possible detector, the following questions should be posed beforehand:

- What spatial resolution is required (pixel size and number)?

  The camera should limit neither the microscope's resolution nor its field of view. Given the total optical resolution of the camera, one should verify that the optical resolution limit of about 250 nm will be sampled sufficiently over several pixels under the high-resolution configuration.
- What temporal resolution is required?

  The acquisition frame rate dictates the temporal resolution of the imaging data. Depending on the scientific question, the temporal resolution of the detector should match either the timescale at which signal changes take place or, at least, the timescale of the stimulus duration.
- What is the expected fluorescence intensity range within a single image?

  The dynamic range of the camera chip and the bit-depth of the collected signal need to be high enough to cover the different intensity levels of the biological sample. A 12-bit resolution is the absolute minimum; a 16-bit resolution chip is to be preferred.
- Is there a need to resolve extremely low signals?

  In this context, the quantum efficiency of the camera chip comes into play (i.e., the probability of detecting single photons). It is important not to focus on the advertised peak quantum efficiency (QE), but rather on the QE in the spectral region of interest. Cameras tend to show a drastic decrease of

this efficiency in the blue, but modern phosphors-based coatings allow pushing the QE up to 70–80%. In low-intensity imaging, additional noise sources must be reduced. One possible strategy to overcome such limitations is to cool the CCD chip, which reduces the thermal noise and is available in combination with several commercial detectors.

Experimental Control

Imaging functional lateralization is a complex process, and many experimental parameters, inside and outside the microscope, need to be controlled precisely. Therefore, a versatile microscope software should meet the following criteria:

- It should allow automatized acquisition in the most flexible way.
- Parameters of the light source and camera should be controllable and included in a configuration file.
- The main computer should have signal input and output ports to synchronize additional devices. A trigger input should allow remote starting of the process, and a frame clock output should allow synchronization of accessory devices (e.g., stimulators) with single image acquisitions.
- The image file format should be as universal as possible and should be readable by third-party software. This will simplify advanced image processing, which always needs to be performed using external programs (Matlab, Python, R, ImageJ, etc.)

2.4.2 Two-Photon Microscopy

Pros and Cons

Two-photon excitation laser scanning microscopy was first implemented in 1990 [62] and, 33 years later, optical neuroimaging would be unimaginable without it (Fig. 4). The fact that the two-photon absorption is limited to the high-intensity region at the focal point has several important consequences, i.e., intrinsic three-dimensional resolution, limited photo-damage, and photobleaching. In addition, because the two-photon excitation resonances are in the near-infrared, the light can penetrate deeper into the sample than the corresponding single-photon excitation light. This allows imaging down to 0.5 mm of depth, granting optical access to most parts of many insect brains.

Its main disadvantage is the high cost. To achieve peak intensities as required for two-photon excitation, ultra-short pulsed lasers are needed. Although new technologies are entering the market, reliable lasers providing these pulses are still expensive. Moreover, the main advantage of the method, its high axial resolution, has a negative side effect in that any motion artifact within that resolution regime is detected and affects the quality of specific signals. Finally, the two-photon elicited signals are of very low intensity, and this should be compensated by using high-efficiency detectors. For this reason, the experimental stage needs to be carefully isolated from any external light sources.

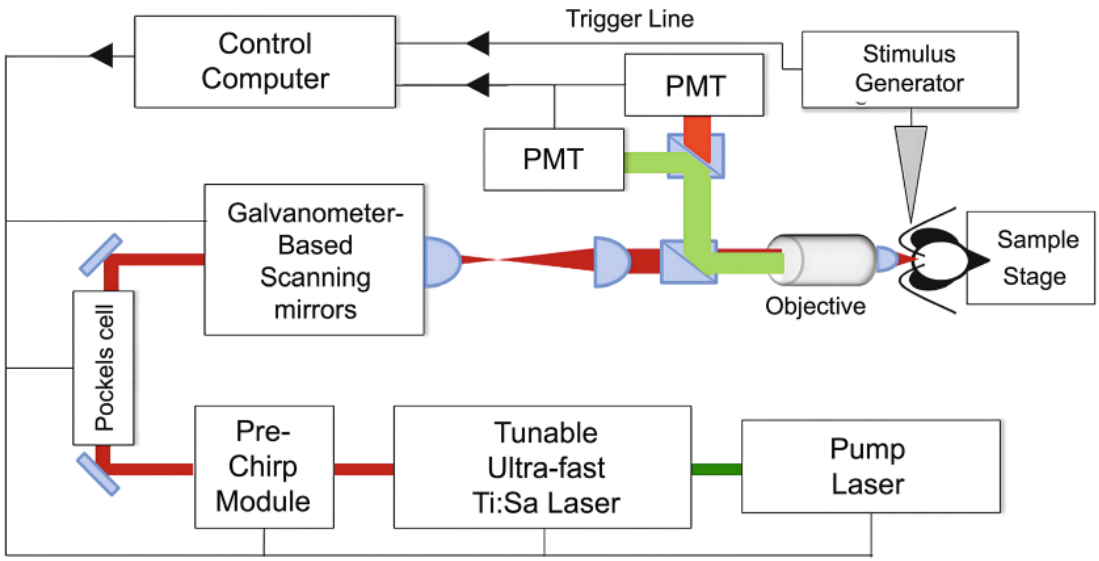

Fig. 4 Schematic setup for functional imaging: a Ti:Sa Laser provides ultrashort pulsed light. A Pockels cell controls the beam intensity. Transversal scanning is achieved by two galvanometric mirrors. Light is then focused onto the sample via an objective with a high numerical aperture. Fluorescence is collected in epi-configuration by the same objective, separated from the backscattered excitation light by a dichroic mirror, and further filtered before being sent to two photomultiplier detectors. A computer controls all elements of the microscopy setup and synchronizes the acquisition with external processes, such as odor stimulus generation. (Reprinted from [120] with kind permission of the Società Italiana di Fisica)

Light Source

In order to excite efficiently two-photon fluorescence in a living sample, the highest possible peak power, which determines the excitation probability, in combination with the lowest possible average power, which is responsible for photo damage, is needed. For this reason, adequate light sources are ultra-short pulsed lasers with a pulse length not exceeding a few hundred femtoseconds (10^{-15} s). The classical solution is a Titanium:Sapphire laser, which can be tuned between 690 nm and 1040 nm. An alternative is the single wavelength Nd:YLF laser, with the drawback of being fixed to a single wavelength of 1047 nm. Recently, interesting new solutions have entered the market, such as erbium- or ytterbium-doped fiber lasers, which promise to be more compact, more robust, and less expensive than conventional lasers.

Pulse length is a further critical aspect: The shorter the pulses, the less average power is needed. However, short pulses will undergo dispersion along the optical path, especially through the objective, causing the pulses to spread. Therefore, an important component of the system is dispersion pre-compensation, a feature that is commonly integrated with commercial systems. Finally, fast intensity modulation of the laser source is necessary to move quickly between different excitation wavelengths, and it is usually performed with a Pockels cell.

Microscope Configuration

Nowadays, two-photon microscopes are available from a large number of providers and with countless options to choose from. Some parameters are dictated by the biological sample. For instance, when imaging a whole insect brain, an upright microscope in epifluorescence configuration is needed. A choice that needs to be made is whether the sample can be positioned on a movable stage, or if the microscope should be movable with respect to a fixed sample (Fig. 4).

Scanning

A fundamental choice is the lateral scanning modality, which usually falls among one of three options: a pair of directly controllable galvanometric mirrors (one of which can be driven resonantly), acusto-optic modulators (AOMs), or spatial light modulators (SLMs). While the singly addressable mirrors are very flexible regarding scanning traces, they provide the slowest option. Resonant mirrors allow fast 2D scanning but with no control on the scanning patterns. The freely addressable and almost instantaneous switchable AOMs allow the so-called random-access microscopy, where several points can be imaged almost instantaneously with fast repetition rates. Spatial light modulators are a flexible solution that allows the generation of arbitrary intensity patterns via phase modulation in the conjugate plane, thus permitting the simultaneous excitation of different regions in a "scan-less" fashion. In the scan-less mode, spatial resolution has to be provided by the detector.

While galvanometric mirrors are the standard option, AOMs should be considered if transient dynamics need to be resolved, and if the molecular markers in use provide a time resolution that matches the one of the scanning process. Spatial light modulation is the newest technique, and it is only about to be introduced into commercial products.

The authors' setup allows switching between freely and resonantly scanning Galvo-mirrors. Using a galvanometric setup, functional images can be acquired by repeatedly scanning custom-defined 1D traces, with scanning rates up to 140 Hz for traces of 256 pixels. Resonant scanning allows for 2D frame rates of 60 Hz for 256 × 256 pixels images, or 15 kHz for straight 1D line-scans. Recently, calcium imaging of AL glomeruli was acquired at 127 Hz for 64x64 pixel resolution [59, 63]. By adding a piezo-driven axial scanner, a full 3D functional image with 256 × 256 × 10 voxels can be achieved at a 5 Hz sampling rate.

Objective

As for widefield microscopy (*see* subheading "Optics"), a fundamental choice is the objective. Here, a high numerical aperture is even more important because the two-photon excited signal has a low intensity and as much light as possible should be collected. Additionally, the objective should be able to correct chromatic aberrations over a wide range of wavelengths (i.e., from infrared to blue), because the excitation wavelength can reach up to

1300 nm, and fluorescence light is collected in the visible region of the spectrum down to 400 nm. Most of them are water-immersion objectives, which makes them compatible with in vivo brain imaging, and reaching numerical apertures up to 1.3. The authors use a 20× (NA = 1.0, Olympus) or a 16× (NA = 0.6, Leica) water-immersion objectives to image single honeybee antennal lobes. In *Drosophila*, a 40× is best suited for AL imaging.

Filters

In two-photon microscopy, color filters are needed for four different purposes: (1) to separate the fluorescence from the back-scattered excitation light, (2) to split fluorescence between different detection channels, (3) to limit the bandwidth of the single channels, and (4) to protect the sensitive detectors against residual laser light. In particular:

- The dichroic mirror, which reflects the fluorescent light toward the detector, is a shortpass filter with a cut-off wavelength just below the lowest excitation wavelength of the laser. Using a Ti:Sa laser, whose tuning range starts from 690 nm, a cut-off wavelength of 660 nm is an appropriate choice.
- A standard way of separating the elicited fluorescent signal is to split it into a green and a red channel. This can be achieved with another dichroic beam splitter and bandpass filters in front of the detectors. The authors use one detection window centered at 525 nm, with 70 nm bandwidth, and a second one centered at 607 nm, with 45 nm bandwidth.
- Finally, the detector arm should host another bandpass filter to block residual laser light, in our case centered at 530 nm with 120 nm bandwidth.

Detector

Two-photon microscopy is a laser scanning technique in which the detector does not need to acquire spatial information but should maximize fluorescent signal collection while limiting background noise. Available options in this regard are photomultiplier tubes (PMTs), or avalanche photodiodes (APDs). Photomultipliers are the most frequently used devices, with high quantum efficiency and very low noise. Their main drawback is their bulky size and the high voltage requirement (1000 V). Avalanche photodiodes can compete with the PMTs in terms of quantum efficiency, but they have a relatively small active area, which requires, for example, de-scanning the beam. The authors use photomultiplier tubes from Hamamatsu and HyD detectors from Leica LSM SP8. With the latter, single photons are registered individually as binary events and continuously read out at 40 MHz, thus providing better sensitivity and a larger dynamic range.

Experimental Control

All points highlighted in subheading "Experimental Control" apply also for two-photon microscopy. In addition:

- Acquisition modes should be flexible, allowing the choice of the dimensionality and directions of the scans. They should allow to restrict the scanning to regions of interest and freely choose exposure times and scanning rates.
- The availability of different scanning modalities—like line scans, spiral scans, or custom-defined traces—is of great advantage.

Laboratory Infrastructure

Three problems we have already mentioned make a two-photon imaging experiment much more demanding than wide-field microscopy:

- The general intensity of the fluorescence signal is low and requires sensitive detectors. This also implies that the experiment must be completely shielded from external light sources, so a lightproof housing has to be built around the microscope.
- Due to the high spatial resolution, laser scanning microscopes are highly sensitive to mechanical movements. Thus, it is necessary to uncouple the microscope from the oscillations of the laboratory floor with an actively air-damped optical table.
- The high laser intensity required for two-photon excitation demands great care regarding laser safety. The utilized lasers are of class IV, and a complete shielding of the laser beam along the entire optical path is highly recommendable.

2.5 Data Analysis

2.5.1 Raw Data Correction

The time-dependent fluorescent signal is usually acquired in the form of a series of 2D images (xy by t). Alternatively, in laser scanning microscopy, temporal resolution can be enhanced by limiting the scanning to a single curve of arbitrary shape. This produces a time series of 1D lines, which can be collectively visualized as a 2D image (x by t). With both approaches, the measure of interest is provided by the stimulus-related change in fluorescence with respect to a baseline signal ($\Delta F/F$). For this, a baseline F is needed, which can be calculated by averaging over several frames (2D or 1D) from the pre-stimulus phase.

In fluorescence imaging, the main signal processing operation is the signal baseline subtraction. Indeed, drifts of the fluorescence signal over time can greatly affect the observed fluorescence. There are essentially two approaches that correct for this effect. The first is a dynamic approach, in which a lowpass filter is applied to the data to average out all activity-induced fluctuations. This provides a dynamic baseline, which is afterward subtracted from the data. The second is a static approach, more laborious but often more precise. In this case, the experiment is fractionated into windows encompassing the single stimulus and its pre- and poststimulus

periods. Then, a linear interpolation is performed between pre-stimulus and poststimulus periods and subtracted from the data in the window. If no significant drift is observed, it is also possible to calculate a static baseline by averaging a few pre-stimulus frames and subtracting this value from the stimulation window [64].

An important aspect is the correction for photobleaching. After a certain number of excitation and emission cycles—which depend, e.g., on the fluorophore, excitation power, and exposure time—fluorescent dyes will reach a nonfluorescent state. In widefield and confocal fluorescence microscopy, it is an important issue because large parts of the sample are continuously illuminated. Conversely, in two-photon microscopy, bleaching effects are usually negligible because of the reduced excitation volume. A correction for fluorescence photobleaching consists of fitting an exponential function to the data to be used for baseline subtraction or by running an experiment without a stimulus to use as a baseline.

Further corrections of these data may be needed in the presence of motion artifacts. In conventional fluorescence imaging, these are mostly movements transversal to the optical axis since motions along the z-axis are usually averaged out due to the limited z-resolution. These corrections can be performed by registering consecutive frames via affine transformations. In confocal and multiphoton microscopy, movements along the z-axis produce a bright/dark modulation (resulting from a moving focal plane) which is hardly distinguishable from an activity signal. In this case, the best strategy is to look for correlations of these modulations across functional units, which would be specific to these motion artifacts. Correction against high-frequency vibrations, instead, can be achieved by lowpass filtering temporal and spatial data.

2.5.2 Functional Data Analysis

For a higher level of data processing, signals have to be associated with single functional units. This can be done by manually selecting regions of interest following the glomerular structures in the images. While two-photon microscopy provides relatively good contrast between single glomeruli, in widefield imaging, boundaries among anatomical structures are often unclear. Therefore, it can be helpful to conclude the functional imaging session with an additional high-resolution image acquisition, which can be used for morphological reconstruction and for assigning functional data to specific anatomical structures. This is also useful when paired with high-frequency multiphoton imaging analysis, an experimental approach that relies on fast scanning rates but is limited in spatial resolution. Another way to isolate independent functional units is to calculate glomerular boundaries by analyzing cross-correlations between the functional data of neighboring pixels [65], or by unsupervised Voronoi tessellation-based image segmentation [66].

Principal Component Analysis

The analysis of spatiotemporal stimulus representation across a population of functional units (e.g., neurons and glomeruli) is a multidimensional problem and requires analytical methods that can take into consideration all available data dimensions. One way to reduce the dimensionality of the problem is to rely on the principal component analysis (PCA). Principal component analysis transforms many possibly interlaced factors into a reduced set of linearly uncorrelated variables, the principal components (PCs). The dimensions of the transformed coordinate space are formally still the same, but now single components are ordered according to their contribution in describing the system's variance, and all are orthogonal to each other, so that there is no redundancy in information anymore. The first component has the highest influence on the variance, the second the next highest, and so on. In systems such as a neuronal network, where single nodes are strongly correlated, the contribution of the principal components decays rapidly with their order. This allows reduction of the dimensionality of the problem by restricting the analysis to the first 2 or 3 PCs, while still describing most of the system's dynamics. These principal components become the new coordinate system for describing the activity signal observed so that odor-specific patterns of response in the AL can be plotted as a function in 2 or 3 Cartesian coordinates of space.

Principal component analysis can be used to explore different types of datasets. For instance, it may be of interest to observe how the representations of various odors diverge over the course of an olfactory stimulation and which is the moment of maximal separation between the odors. For this analysis, odor response trajectories are plotted throughout different time points as a function of the principle components (Fig. 5).

Euclidean Distances

When handling odor response data from a large subset of glomeruli, a multiple comparison analysis has the drawback of increasing the family-wise error rate, and differences between single glomeruli may be lost. The highest possible compression of the information regarding the similarity between two stimuli can be achieved by computing their Euclidean distance. Briefly, the response intensity of each glomerulus is considered as a single dimension, and an odor is represented by a vector of values in an n-dimensional space, where n is the number of considered glomeruli. The difference between two odorants can then be described by the distance between these two vectors. When x_i and y_i are the responses relative to odor x and odor y within glomerulus i, the Euclidean distance $d_{x,y}$ is given by

$$d_{x,y} = \sqrt{\sum_{i=1}^{n} \left(x_i - y_i\right)^2}$$

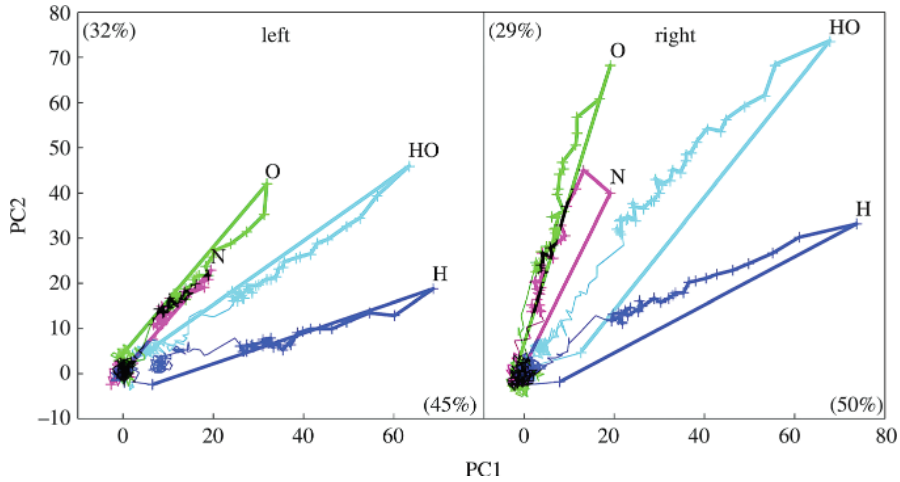

Fig. 5 Trajectories of the odor responses in all glomeruli of left ALs (426 glomeruli) and right ALs (455 glomeruli) were calculated using PCA. Crosses represent values for subsequently sampled frames during olfactory stimulation (125 ms inter-frame interval). Higher distances between activation vectors in the right AL indicate greater inter-odorant distinguishability. (Reprinted from [68] with permission from The Royal Society)

Euclidean distances can also be calculated at various time points in the experiment to monitor how differences between odors are building up in the AL across time. In general, the Euclidean distance is the best quantitative way of analyzing the distinguishability of two odorants across the AL glomeruli. It has also been demonstrated that such an estimate of distance correlates well with the perceived similarity/dissimilarity of the same two odors in a behavioral paradigm [67].

2.6 Results and Perspectives

2.6.1 Honeybee

The first results of comparative imaging of odor codes in insects were obtained by Galizia et al. in 1998 [12] using a Calcium Green-2-AM bath application. The resulting signals comprised calcium changes across different cell populations, such as olfactory receptor neurons, local interneurons, projection neurons, and glial cells. For imaging, they used a conventional fluorescent microscope equipped with a 40×, NA 0.6 LD air objective and a cooled CCD camera (Photometrics CH250A). Odor responses were acquired with a spatial resolution of 51 × 51 pixels (binned on chip from 512 × 512 pixels) over a field of view of 250 × 250 μm, which allowed imaging of the superficial layer of single antennal lobes. Morphological information on the glomerular structure was obtained by counterstaining the bee brain with the membrane dye RH795, and by imaging the whole brain with a 5× objective. Statistical tests on the functional response pattern of left against right antennal lobe to 13 volatile compounds in 30 glomeruli showed no significant asymmetries between sides ($n = 25$ bees).

This lack of asymmetry was confuted by a more recent study by Rigosi et al. [68] conducted with a similar optical setup, a widefield

fluorescence microscope Olympus X-50WI with a water immersion objective (20×, NA = 0.95, Olympus), and a CCD camera (Imago QE, Till Photonics). The spatial resolution was 172 × 130 pixels over a field of view of 300 μm. In this case, AL projection neurons were selectively backfilled with Fura-2-dextran. Calcium signals were temporally resolved with a 10 Hz, which allowed a more detailed analysis of the response signal dynamics. This analysis was based on 33 bees, with 8–20 identified glomeruli per individual. Measuring the Euclidean distance across odor representations between left and right AL allowed the detection of significant lateralization within the odor response patterns. The code showed a better distinguishability of olfactory stimuli within the right antennal lobe.

2.6.2 Fruit Fly

Louis et al. [69] found an asymmetry in chemotaxis in *D. melanogaster* larvae, i.e., a difference in performance between animals with just left or right functioning olfactory receptor neurons (ORNs). Besides the finding that the overall accuracy of navigation in odor gradients is enhanced by bilateral sensory input, they showed that a right-functional-ORN animal displayed a significantly better chemotactic behavior than the corresponding left-functional animal. Behavioral experiments were performed blindly with respect to the expression type, which was determined after each experiment by removing the anterior tips of larvae, fixing the brain, and imaging it in confocal microscopy (*see* Subheading 3.2.3). Nonfunctional ORNs were tagged with a red fluorescent protein (RFT), and functional ORNs with GFP. The imaged volume was projected in a single 2D image to evaluate the overall GFP expression, which allowed the identification of the functional ORNs. The observed hypersensitivity shown on the right side was explained by differential gene expression levels, suggesting that this lateralization is an innate feature of the insect brain.

2.6.3 Perspectives

While the observed functional effects represent proof for the existence of some degree of lateralization in the antennal lobes of insect brains, the possibilities offered by modern fluorescence imaging are far from being fully exploited. So far, odor response signals are averaged over all projection neurons afferent to the same glomerulus, and its calcium signal intensity is a measure for the odor code. In vivo application of two-photon microscopy offers a spatial resolution that allows resolving single neurons and sub-cellular structures and a temporal resolution that may resolve single action potentials. Furthermore, the optical access provided by two-photon microscopy enables the investigation of sub-surface brain regions, such as honeybee PNs belonging to the T2-T4 tracts, regarding possible functional asymmetries.

3 Ex Vivo Imaging

3.1 Preparation: Methods for Immunohistochemistry

Structure accessibility and staining specificity limit in vivo imaging analysis. The study of the nervous system via classical and immunohistochemical techniques has always been adopted to complement in vivo optical and electrophysiological recordings, as well as behavioral experiments. In the following paragraphs, we will introduce the main histological methods used to investigate lateralization in insects' central nervous systems, from tissue handling, preparation, and staining, to image acquisition, and we will discuss the main issues of data analysis.

3.1.1 Tissue Handling

Careful brain dissection and proper tissue handling are crucial steps for any anatomical and histological analysis. Insect brain tissue should be dissected with the appropriate care in phosphate buffer saline (PBS) or insect Ringer solution [70]. The operation should be conducted at 4 °C, in order to delay the degradation processes triggered by anoxia and stressful conditions. After a quick dissection phase, the brain tissue is placed in the fixative solution [70]. Alternatively, the whole head capsule may be fixed overnight prior to brain dissection [71]. This step may facilitate the dissection process and preserve the original size and proportion of brain structures [16]. A standard protocol for fixation of the honeybee brain consists of a 12/24-hour incubation of the tissue in 4% PFA in PBS at 4 °C under slow shaking on a bench rocker. For the fruit fly's smaller brain, 1 hour is commonly sufficient [72]. Afterward, the tissue can be stored at 4 °C in PBS indefinitely.

3.1.2 Tissue Labeling

Brain labeling for imaging analysis can follow two distinct approaches: the tissue can be analyzed in the whole mount (i.e., the brain structure is conserved intact) or sliced. The first approach, normally discarded for bigger-sized brains, becomes very efficient when working with miniature insect brains. In fact, their limited thickness makes them more easily accessible to antibody staining and optical imaging. This approach becomes particularly effective when coupled with confocal or two-photon microscopy, as both optical techniques provide high 3D resolution. Alternatively, brain tissue can be sliced into 5 to 20 μm-thick sections. The latter method is more laborious than the former one, but it offers some advantages. First of all, working on thin sections eliminates the need for a confocal or two-photon microscope for the imaging process. In addition, both fluorescent and nonfluorescent markers can be employed for labeling, allowing the use of bright-field microscopy (Subheading 3.2.1). Also, antibody labeling improves in these conditions due to a higher level of exposure to the target epitopes. Finally, neighboring sections can be stained with different markers, allowing a virtual multiple-staining approach, a

methodology that is limited by the microscope's optical filter setup and by antibody specificity when working in whole mount configuration.

In both cases, a permeabilization treatment is required to allow the primary antibody to penetrate the tissue and reach the target antigen. Tissue permeabilization can be achieved by incubation with a detergent, which will partly dissolve cellular membranes making the various cell compartments accessible to labeling. Detergent concentration and duration of the treatment are variable and need to be optimized case by case. Protocols vary from a 10-minute incubation with 0.1–0.2% of Triton-X100 in PBS to a higher concentration (0.5% in PBS) and longer tissue exposure time (30–60 min) when milder substances such as Tween-20 are used. Before the primary antibody incubation, all accessible nonspecific epitopes should be blocked to prevent the nonspecific binding of the antibody. This can be obtained by incubating the tissue in a 5–10% solution of normal serum in optimized conditions of duration and temperature (i.e., a time window ranging from 30 min at room temperature to 24 h at 4 °C, based on the used primary antibody). Normal serum is rich in antibodies that will bind to endogenous targets, thus preventing the nonspecific binding of both primary and secondary antibodies used in the assay. For this step, it is important to use a serum from a different animal species than the one, in which the primary antibody was raised. Otherwise, the secondary antibodies recognize and bind the antibodies present in the blocking solution along with the primary antibodies bound to the target antigen.

After the permeabilization and blocking steps, the tissue is ready for immunolabeling. Direct immunolabeling is achieved using a labeled antibody, which binds directly to the target protein. Alternatively, indirect immunolabeling can be performed using two types of antibodies: the first one (primary antibody) is not labeled and recognizes the target epitope, while the second one (secondary antibody) is labeled and specifically targets the primary antibody. This method has two major advantages with respect to direct labeling. The first one is that it amplifies the signal because several secondary antibodies can bind to a single primary antibody. The second consequence is that it allows using commercial secondary antibodies already labeled with the desired probe. The same secondary antibody will interact with any specific primary antibody of a given species. For these reasons, indirect immunolabeling is generally the standard approach adopted in immunohistochemistry. Labeling is highly dependent on the antibody used, both in terms of concentration (from 10^{-2} to 10^{-4}; indications are usually provided by manufacturers) and incubation time (from a few hours to several days). Whereas the antibody concentration needs to be tested for each batch of product, a 3-day incubation period at

4 °C is usually appropriate. After washing the tissue to eliminate the excess primary antibody, the labeling procedure continues with a more standard exposure to the secondary antibody (also in this case, a starting duration of 3 days is advised). Afterward, a few quick washes (e.g., 3 × 20 min washing) are performed to wash away the antibody in excess. If the secondary antibody is fluorescently labeled, the brain tissue is then ready for visualization. If it was cross-linked to an enzyme requiring a chromogenic substrate for bright-field microscopy visualization, the tissue is now ready to be exposed to the substrate for signal development. These two different labeling approaches are described briefly in the following paragraphs.

3.1.3 Probes

Fluorescent Probes

As discussed in the previous paragraphs, immunohistochemistry can be conducted with both fluorescence and bright-field microscopy, and the probes will need to be selected according to the choice of imaging setup. To date, fluorescence microscopes are readily available in the majority of research facilities, and the use of fluorescent imaging for specific visualization of cellular compartments has become standard practice. A wide choice of fluorescent probes is available from different manufacturers matching a wide range of excitation wavelengths, from UV to red light (*see* Table 1). An appropriate combination of excitation, dichroic, and emission filters on the imaging apparatus will easily allow multiple labeling on the same tissue without signal overlapping [70, 73, 74]. Importantly, prolonged excitation of a fluorescent molecule will eventually lead to signal bleaching. However, compared to the first organic dyes (e.g., Fluorescein/FITC, or Rhodamine), the more recently developed ones (e.g., Alexa, or Cy families) show a much higher photostability [75]. Moreover, state-of-the-art fluorescent probes yield a much brighter signal due to higher resistance to self-quenching effects (i.e., when fluorescent molecules form complexes that are not excitable anymore).

Fluorescent labeling is intrinsically sensitive to light exposure. Therefore, all procedures involving fluorescent probes should be carried out in the dark or under illumination that does not excite the markers (e.g., yellow–red). In this respect, the sample must be protected from light during fluorescent antibody labeling by keeping it inside a dark box or in a dedicated room. Concerning sample storage, fluorescently labeled samples can be stored for several months at 4 °C in the dark.

The development of superresolution imaging triggered the development of new dyes that can be used for various fluorescence imaging applications but which excel in specific superresolution techniques such as stimulated emission depletion (STED) microscopy [76]. For studying synaptic distribution in honeybee MB

microglomeruli (MG), the authors adopted the Abberior STAR RED antibody for STED imaging [77].

Nonfluorescent Probes

Alternatively, immunohistochemistry can be conducted in bright-field microscopy by employing secondary antibodies cross-linked to enzymes such as horseradish peroxidase (HRP) or alkaline phosphatase (AP). These enzymes are not directly detectable but catalyze the conversion of a chromogenic substrate into a colored precipitate, which will indirectly indicate the localization of the antibody-labeled structure. For instance, in the presence of hydrogen peroxide applied as an oxidizing agent, HRP oxidizes diaminobenzidine (DAB), turning it into a dark-brown precipitate. Similarly, AP catalyzes the hydrolysis of a phosphate group from the substrate molecule of choice, resulting in a colored product. Importantly, chromogenic substrates are intrinsically sensitive to oxidation, and brain tissue is rich in peroxidases that can quickly oxidize the substrate producing a strong background signal. Hence, before incubation with enzyme-labeled secondary antibody, tissue should be treated with a saturating amount of hydrogen peroxide (e.g., 0.3% H_2O_2 in TBS or PBS for 15 min) to achieve irreversible inactivation of endogenous peroxidases and reduce the nonspecific background signal.

Various chromogenic substrates have been developed, allowing HRP and AP (or other enzymes) to generate reaction products with different chromatic properties. This offers the possibility of conducting multiple labeling experiments on the same tissue and pairing any labeling with the counterstaining of choice. Nonetheless, when dealing with spatially close or overlapping signals, it must be considered that this method is less reliable than fluorescent probe labeling in terms of signal discrimination and co-localization analysis [78]. Also, signal intensity cannot be used as an estimator of the amount of the conjugates present in the sample because it can be significantly affected by the developing time (i.e., the period in which the enzyme operates on the substrate). This may vary from a few seconds to several minutes according to tissue properties, labeling efficiency, enzyme, and substrate quality. An advantage associated with nonfluorescent labeling is that the colored product of the oxidative or dephosphorylation dephosphorylation enzymes is permanent and stable in time and is unaffected by light exposure. Hence, immunolabelled sections can be stored at room temperature indefinitely, with no effect on staining quality. Finally, the use of nonfluorescent probes can be coupled with several classical methods of histological staining, developed during the pre-fluorescence imaging era and still routinely used for their simplicity and the reliability of the developing process (for an extensive review of the most common reagents for histological counterstaining, *see* [78]).

3.2 Image Acquisition

Imaging methods for fixed tissues are technically less demanding compared to in vivo imaging analysis. Within this section is to introduce bright-field microscopy briefly and to compare the two 3D fluorescence microscopy techniques, regarding their benefits in anatomical imaging of insect brains.

3.2.1 Bright-Field Microscopy

Bright-field microscopy is the simplest of all forms of microscopy. The specimen is illuminated from below if transparent or, if not, from the side (or above). While this method is largely used for animal preparation and histological analyses, quantitative measurements are nowadays mostly based on fluorescence microscopy. Nevertheless, it is worth mentioning that one should consider the following points before buying a bright-field microscope to perform insect brain imaging.

Magnification Range and Working Distance

The magnification can be changed within a certain range by adjusting the microscope tube length, i.e., the distance between the objective and the ocular lenses. One should ascertain that the chosen magnification range allows a full view of the sample mount and that it allows zooming into specific brain centers to identify structures of interest. Also, whenever manipulation of the sample is supposed to happen under the microscope, a comfortable working distance (e.g., 10 cm), which is the distance between the sample and the objective, is needed.

Illumination

For manipulation of the sample under the microscope, a light source with the smallest possible angle against the optical axis should be chosen in order to avoid shadows due to hands or instruments during dissection and manipulations. Traditionally, flexible light guides represent the best solution. Nowadays, rings of LEDs can be mounted around the objective, and they provide a valid alternative. If fluorescent samples are prepared under the bright-field microscope, an illumination out of the excitation window of the markers is advised to prevent photobleaching.

Camera

In bright-field microscopy, image or video recording is often needed. While the easiest and cheapest solution is mounting a camera onto one of the eyepieces, a useful alternative is recording via camera while monitoring the sample via both eyes. In this case, one should consider buying a trinocular microscope with a camera port, through which the signal can be split between camera and binoculars. Otherwise, it is possible to employ a transparent CCD camera, to be integrated into the optical path. The latter solution is more flexible, but also more expensive.

3.2.2 Widefield Fluorescence Microscopy

Thanks to its accessible costs, widefield fluorescence microscopy is the method of choice for the analysis of tissue slices, which do not need 3D resolution. Regarding the design of the imaging setup, the points discussed in Subheading 2.4.1 remain valid. In Table 1, some of the most used fluorescent probes are listed, together with their spectral properties, i.e., excitation and emission wavelengths, as well as the cut-off wavelengths suggested to separate the fluorescence from the excitation light. As soon as the samples become thicker (>10 μm), the need to suppress off-focus fluorescence to obtain a reasonable image contrast will strongly favor confocal or two-photon techniques.

3.2.3 Confocal Microscopy

Confocal microscopy is an extension of the widefield fluorescence method, in which only the light from a single focal plane is allowed to reach the detector. This is achieved by a post-selection operated by a pinhole placed in the confocal plane, i.e., the conjugated plane to the focus in the detector pathway of the microscope. Adjusting the pinhole size allows selecting how strict the blocking of off-focus light should be. This not only controls the axial resolution but also influences the intensity of the detected signal: a larger pinhole will allow more light to pass through, but such light will be emitted from a thicker confocal plane. Confocal microscopy is a laser-scanning technique, and two-dimensional imaging is achieved by laser scanning one pixel at a time. The third dimension can be added by moving the objective perpendicularly to the sample mount. This implies that many components will be identical or similar to those needed for a two-photon microscope. This has already been covered in Subheading 2.4.2. Therefore, only the differences will be highlighted in the following paragraphs.

Pros and Cons

Because of its axial resolution, confocal microscopy is the most common technique adopted to investigate the morphology of thick samples. Its advantage over two-photon microscopy is the lower costs of the laser source. do not need to be short-pulsed, as the excitation is here based on single photon transition as in conventional fluorescence microscopy. However, this is also one of the disadvantages of this method. Although light is collected only from the focal plane, absorption happens in the whole light cone, producing strong photo-bleaching effects. A second drawback of confocal microscopy is the fact that the single-photon transitions are excited in the visible range, mostly in the blue or green, while the same transitions would be excited by infrared light in two-photon microscopy. Optical properties of brain tissue are strongly wavelength-dependent [79], and this causes the penetration depth to be at least twice as high in two-photon microscopy (300–500 μm in two-photon imaging of untreated tissue [80]), compared to single-photon excitation.

Light Source

The light source is the component that differs substantially between confocal and two-photon microscopy. To cover the whole spectral window needed for the most common fluorescent markers, multiple laser sources are generally combined within one setup. Typically, five emission wavelengths are sufficient to excite efficiently almost all commercially available probes. Standard solutions combine helium–cadmium lasers (emitting at 325, 353, and 442 nm), argon–ion lasers (488 and 514 nm), argon–krypton mixed-gas lasers (488, 568, and 647 nm), and helium–neon laser (543 and 633 nm). Until now, gas lasers have been the standard solution, but, in the future, they will most certainly be replaced by laser diodes and solid-state lasers, which are more stable, more compact, and easier to cool. A different class of confocal microscopes use multiple-beam systems. Such setups are often equipped with arc lamps from widefield fluorescence microscopy (subheading "Light Sources") to reduce photo damage.

Scanning

The 2D image formation is based on laser scanning, and it is used in the same way as in two-photon microscopy. Hence, the same considerations as in subheading "Scanning" apply. Multiple-beam scanning confocal microscopes are based on a different mechanism. A spinning disk with an array of pinholes and microlenses allows for illuminating multiple points at once, thereby strongly increasing the scanning rate.

Objective

As in other fluorescence imaging techniques, the objective is the most important optical element for the imaging quality (*see* subheading "Optics"). In confocal microscopy, it is important to maximize the numerical aperture of the lens, which increases the focus of the laser beam: the more the laser beam is focused, the more efficiently the post-selection process of the emitted signal from the focal plane works. The optical pathway beyond the objective in confocal microscopy differs slightly from that used in two-photon microscopy. The fluorescence collected in epi-configuration is sent back via the scanning unit to be de-scanned and is then separated from the backscattered excitation light via the appropriate filters. An additional element that we have already mentioned, is the adjustable pinhole in the conjugated plane to the focus, which permits axial selection of the signal before it reaches the detectors. The adjustable size of the pinhole allows one to balance the generated signal between resolution and intensity. The size is measured in Airy units ($1\ \mathrm{AU} = 0.8\,\lambda/2/\mathrm{NA}$), a unit related to the diffraction limit (thus, dependent on wavelength λ and numerical aperture NA). A pinhole of 1 AU (≈ 0.2 μm for $\lambda = 488$ nm and $\mathrm{NA} = 1.0$) usually provides the best signal-to-noise ratio. If the signal is sufficiently intense, the pinhole can be further closed to $\approx$ 0.5 AU to improve spatial resolution.

Filters

The general confocal microscopy setup comprises an excitation filter limiting the bandwidth of the excitation source, a dichroic filter that separates the fluorescence from the backscattered excitation light, and emission filters, which select the spectral detection window. If simultaneous imaging on more than one detection channel is performed, an additional beam-splitter and separate emission filters are needed. Notably, the dichroic filter splitting the emission from the excitation light must be a steep shortpass filter because excitation and emission wavelengths are much closer than in two-photon microscopy, and residual excitation light produces a strong background signal.

Detectors

Since single-beam confocal microscopy is a laser scanning technique, the detector does not have to provide spatial resolution. However, the post-selection process strongly reduces the fluorescence intensity, and high-sensitivity detectors are necessary. Photomultipliers are the most common solution, although avalanche photodiodes can be a more compact alternative if the beam can be focused on the smaller active area. In multiple beam scanning confocal microscopes, the signal has to be spatially resolved by an array detector, such as a CCD or a CMOS camera.

3.2.4 Two-Photon Microscopy

Brain Imaging In Situ

The anatomical imaging of antennal lobes in vivo has the advantage of avoiding artifacts due to tissue isolation, fixation, and dehydration [81]. This is not a common procedure but can be useful when minimum structure alterations due to tissue fixation must be avoided. For enhanced penetration depth, it is recommended to rely on two-photon microscopy. The imaging system is equivalent to the in vivo case, described in Subheading 2.4.2, and filters have to be adapted to the fluorescent markers. For example, in studies measuring glomerular volume, RH795 is used [82], which is excited best at 1040 nm in two-photon microscopy (490 nm in the single-photon case), and has its spectral emission peak at 690 nm.

Extracted Brain

When imaging fixed brain samples, the increased penetration depth of two-photon microscopy can be easily compensated in a one-photon confocal configuration by optical clearing [83, 84]. An efficient preparation for AL morphological imaging is, for example, synaptic staining using an anti-synapsin antibody (Subheading 3.1.2) coupled with a secondary antibody conjugated, e.g., to an Alexa fluorophore.

3.2.5 Emerging Techniques

STED Microscopy

In recent years, optical methods breaking the resolution limits (~200 nm) have become available under the name of super-resolution microscopy methods [85] and allow resolving and quantifying sub-cellular components in a living cell system at a < 50 nm scale [86]. For instance, Stimulated Emission Depletion Microscopy (STED) has been shown to be able to resolve individual

synapses and even sub-synaptic structures [87]. This technique is well suited for insect brain imaging, and a protocol for immunostaining and subsequent STED imaging in *Drosophila* brain slices is available [88]. In vivo, STED has been shown to work in *Drosophila* larvae [89]. In honeybees, STED microscopy has been introduced to resolve synapses within mushroom body microglomeruli [77].

Electron Microscopy

Electron microscopy (EM) was the first imaging method that allowed visualization of the ultra-structure of the insect brain [90]. It was applied for counting synapses in the honeybee AL [91] and provided the first insights into synaptic structures and age-related plasticity [92] in several insect species [93].

In recent years, EM application has been driven by multiple technological developments [94]. The first one is the extension of EM from transmission imaging of single slices to volume electron microscopy (VEM), which allows one to obtain 3D datasets with nanometer resolution. The second one is the development of the data analysis methods that are necessary to cope with such an enormous amount of data. Thanks to these technological upgrades, EM can be used to automatically track single neurons and identify synaptic connections in order to reconstruct the brain's microcircuits. Another advancement is a data acquisition technique known as serial block-face electron microscopy (SBEM) [95]. In this method, an electron beam scans the surface of a sample typically embedded in an epoxy resin and stained with heavy metals, while backscattered electrons are collected to produce the EM 2D image. Following imaging, an ultramicrotome is used to cut a thin section (typically 20 nm) from the face of the block, after which the sample is imaged again.

Reconstructing the connectome can be based on manually supervised neuron tracing assisted by tools for visualization, measuring, and mapping of wiring diagrams from fine dendritic branches to multi-neuron graphs like the Collaborative Annotation Toolkit for Massive Amounts of Image Data (CATMAID) [96]. In other species, like the zebrafish, techniques for automated reconstruction have been implemented [97]. In this case, multiple 3D Conjugated Neural Networks (CNNs) were used to perform a semantic segmentation of the EM volume.

3.3 Data Analysis

3.3.1 Image Segmentation

One of the main approaches in ex vivo analysis is volume reconstruction of anatomical structures based on image segmentation, i.e., the process of partitioning a digital image into multiple regions. The goal is to reduce the information contained in a complex image into something easier to analyze. This is usually achieved by defining clear boundaries of identifiable structure or by setting a threshold that will automatically segregate meaningful signals from the background. When applied to a stack of images, the boundaries defined by the segmentation process can be used to

reconstruct a three-dimensional model of the structures of interest, generally in combination with several smoothing/sharpening and interpolating functions provided by any reconstruction software.

For a reliable 3D reconstruction, it is crucial to obtain a carefully prepared tissue sample, in which the structure of interest is well preserved and evenly stained. Synaptic markers such as anti-synapsin antibodies or, for *Drosophila*, anti-nc82, are preferentially used because they provide homogeneous staining throughout the neural tissue and enhance anatomical structures and neuropils' boundaries [16, 70, 74]. Images should be acquired at high resolution and in stacks with a relatively small step size along the *z*-axis. Due to its accessibility and the interest in lateralization of the insects' olfactory circuits, one of the most studied neuropils has become the antennal lobe. In honeybees, an AL can be correctly reconstructed by imaging with a 20× water immersion objective, and acquiring images at 512 × 512 pixels resolution, in steps of 3 μm along the anteroposterior axis [12, 82]. In the fruit fly, this neuropil is much smaller, and good results were achieved by imaging with a 40× water immersion objective in steps of 1 μm.

Even if this approach is better suited for high-resolution fluorescence microscopy of whole-mount preparations, a first attempt to study lateralization in the honeybee AL was performed on paraffin-embedded 5 μm-thick slices. In that case, the tissue was stained with Luxol fast blue, a histochemical staining that sharply highlights the boundaries of AL glomeruli. Glomerular volumes were estimated using Cavalieri's direct estimator, a stereological technique that allows the estimation of the volume of arbitrarily shaped objects from a set of randomly oriented, parallel histological sections [98].

Two major issues have been encountered in performing fine measurements of volume lateralization. The first problem concerns the quality of 3D reconstruction, and it is strictly dependent on the process of segmentation, the quality of the specimen, and the quality of the acquired images. Segmentation can be done automatically, with a threshold or a watershed algorithm, but the quality of the staining, as well as the presence of disturbing structures (e.g., shadows, tracheas), can influence the reliability of the results. Alternatively, due to the common presence of imperfections in biological preparations, it is possible to conduct the segmentation manually by selecting the boundaries of the anatomical structure of interest in the three orthogonal planes and applying a wrapping algorithm to interpolate the full 3D surface. One solution to identify poor segmentation quality is to vary the starting parameters of the reconstruction procedure. If the outcome is dependent on the starting parameters, the image quality is probably insufficient, and such a dataset should be discarded.

The second issue concerns the high variability of measured volumes across individuals. Volume differences from left to right

side in a lateralized structure may be consistent but also relatively small if compared to inter-individual variability. For instance, the absolute volumes measured on the individual glomeruli of the honeybee AL vary significantly among different individuals. Therefore, it is recommended to directly compare volumetric data from the left and right sides of the brain within a single animal. Such left/right difference can be quantified by a lateralization index $L = V_R / (V_R + V_L)$ where V_R and V_L denote the right and left volume, respectively [82]. Lateralization index L ranges from 0 to 1 around the symmetry point 0.5. This will allow comparison of the degree of lateralization among individuals, without the influence of inter-individual variability.

3.3.2 Quantification of Objects

Brain asymmetries can be quantified by object counting, where "objects" can be any biological structure present in multiple copies in both the left and right brain hemispheres (e.g., receptor neurons, synapses, neuropils, mushroom bodies microglomeruli.). This approach has been used widely to identify brain differences across animals of different developmental stages [99] or subjected to different conditioning procedures [73], but it has not yet been adopted to study anatomical correlates of brain lateralization. This method is suited for both whole brain and sliced brain preparations, stained with both fluorescent and nonfluorescent probes. For instance, Hourcade et al. investigated the density of microglomeruli (MG) in the honeybee mushroom bodies and their relationship with olfactory learning [73]. Microglomeruli are anatomical structures comprising the presynaptic axon terminals of AL projection neurons and the surrounding postsynaptic dendritic spines of MB Kenyon cells. They can be easily identified by double labeling with anti-synapsin antibody (presynaptic site) and phalloidin (dendritic spines). In the study, the bee brain was sliced into 5-μm sections, and two optical sections containing the medial lips and collars of the two medial calyces were considered in each animal for the analysis. Then, a circular area was drawn in each of the regions of interest, i.e., lip and collar of the medial MB calyces, and MGs were individually counted within each circle. This operation can be performed in several regions of interest and across multiple individuals in order to quantify the number and density of the microglomerular structures.

Commercial and open-source image processing software (e.g., Amira, ImageJ) have implemented automated counting tools, allowing quick and high-throughput analysis of several samples in a non-biased manner. However, imperfections in the sample preparation and the lack of resolution may result in processing problems and cause strong deviations of fully automatized approaches from manually obtained results [100]. For these reasons, mixed approaches are often the best choice, namely visually supervising and calibrating the automated tools. Usually, this results in

analyzing multiple relatively small regions of interest (ROIs) inside the target structure. Counts are then averaged across ROIs, and the total number of objects in an area or a volume is extrapolated by multiplying ROI counts with the ratio between ROI area/volume and total area/volume.

Recently, efforts have been made to develop robust automated tools that allow direct counting within larger structures. This approach has the advantage of detecting and visualizing spatial fluctuations in the number or density of the analyzed structures (Fig. 6). A typical problem of the extrapolation from small ROIs is

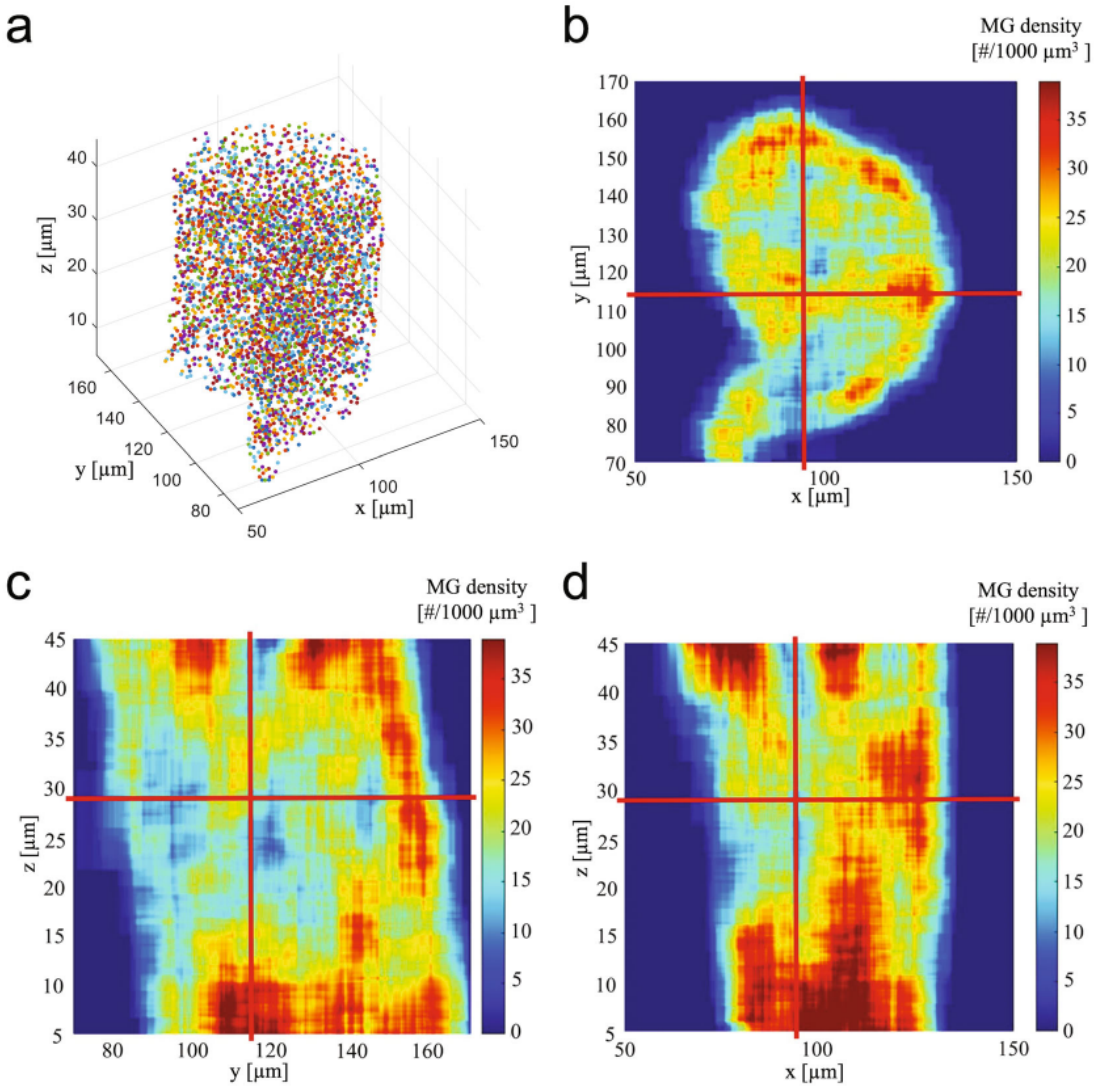

Fig. 6 Spatial distribution of microglomeruli identified within a subregion of the MB lip using an automated method. (**a**) The central coordinates of microglomeruli (colored circles) were used to visualize their 3D distribution in a lip section of 40 µm thickness (random colors for visual discrimination) (**b**-**d**) The density of microglomeruli for 1000 μm^3 was obtained by a running average, using a volume element of that size. This revealed the heterogeneity in the microglomerular distribution in all dimensions of the MB lip. The red lines represent the focal planes used to display all 3 dimensions [101]

the so-called boundary effect of ROI-based analysis. This issue is often ignored or underestimated so that the extrapolated values are frequently an overestimation of what can be observed from a direct count [101].

3.3.3 Fluorescence Intensity Measurements

A third quantitative approach that can be used to compare bilateral brain structures is the analysis of fluorescence intensity. This method relies on the fact that the intensity of a non-saturated fluorescent signal is directly correlated with the number of antigens available for labeling, representing an indirect measure of the amount of the target molecule present in the sample. To our knowledge, this approach has been routinely used to address other biological questions [99, 102, 103], but has not been applied to the study of brain lateralization yet. When dealing with fluorescence intensity quantification, it is important to consider that the preparation of different samples may vary in terms of background autofluorescence and labeling intensity. Therefore, signal quantification should be measured with respect to a reference intensity rather than as an absolute value, e.g., relative to the mean fluorescence of the analyzed structure or relative to the background signal. When the research hypothesis is probing the relative change between two structures after a certain treatment, the difference in fluorescent signal can be optimally quantified as the ratio between the signal intensity of the two structures before and after treatment [104]. This last approach is very powerful in highlighting subtle differences linked to brain lateralization. For our purpose, an approach that measures directly the ratio between left and right structures (such as a certain glomerulus, or the microglomeruli of a specific mushroom body area) will enhance any small but consistent differences in the expression of a given epitope. On the contrary, an approach in which the fluorescence intensities of the investigated structures are normalized against a reference value prior to a direct comparison could flatten a potential difference between signal intensities.

3.4 Results and Perspectives

3.4.1 Honeybee

Standard Atlas of the Bee Brain

The basis for all anatomical lateralization studies in insect brains is standard atlases, which, by means of specific landmarks, allow the identification of individual functional units. The first 3D model of the honeybee antennal lobe was constructed by Flanagan and Mercer in 1989 [105] via phase-contrast bright-field microscopy. Brains were fixed, dehydrated, paraffin-embedded, and cut into 10 μm-thick serial slices. Retrograde injection of cobalt chloride was used to stain cells, and histological sections were then digitized and 3D-reconstructed. The first high-resolution digital atlas of the antennal lobe was created by Galizia and colleagues in 1999 [15] using confocal microscopy. The ORN axons were traced via neurobiotin and stained with Cy3-conjugated streptavidin injected via the antennal nerves. Brains were then fixed and imaged using a

Leica TCS 4D with an LD 16× oil-immersion objective (NA = 0.5). As a light source, they used a 568 nm line of an ArKr 150 mW laser, and fluorescence was filtered by a long pass 590 nm filter. The labeling resulted in clear fluorescent staining of the glomeruli, and the use of confocal microscopy allowed the entire AL to be scanned as a whole mount, with no need to slice the preparation (Fig. 7). The resulting atlas provides a clear three-

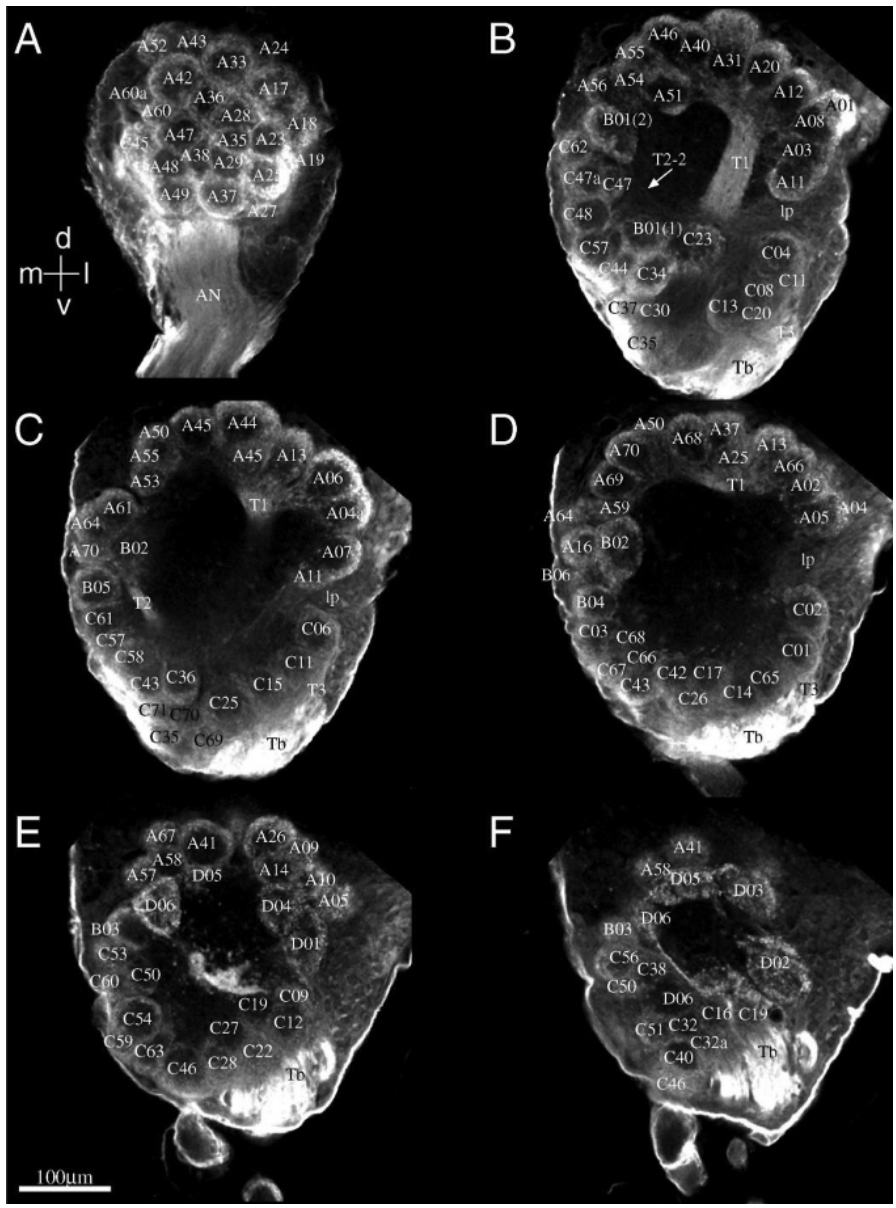

Fig. 7 A series of six confocal optical horizontal sections (**a**) 26 µm, (**b**) 78 µm, (**c**) 104 µm, (**d**) 130 µm, (**e**) 169 µm, (**f**) 195 µm) of the honeybee left AL in which ORNs' axons were fluorescently stained. Individual glomeruli are labeled. (Reprinted with kind permission from Springer Science+Business Media [15])

dimensional grid for the glomerular positions with improved resolution (2.4 μm axial slice distance and no loss of information between them, so that no glomeruli are missing).

Later, Brandt and colleagues created the first common spatial reference map of the entire honeybee brain [106] via confocal microscopy. Preparations and imaging techniques were identical to those of Galizia et al. [15], except for the fact that a Leica HC PL Apo × 10/0.4 dry objective had to be used to increase the field of view. The standard atlas was calculated from multiple individuals by averaging the shape and size of all brain areas and applying an intensity-based nonrigid registration algorithm. Notably, the bee brain atlas is available on a public platform together with other insect brain atlases and is continuously updated with newly characterized neurons [107].

Comparative Volume Measurements

Winnington et al. [98] published the first results on comparative volume measurements in the honeybee brain using bright-field microscopy. Brains were extracted, fixed, paraffin-embedded, and sectioned into 5-μm-thick slices. Sections were stained either with Luxol fast blue/cresyl violet, hematoxylin and eosin, or by cobalt chloride backfilling of antennal sensory afferents and Timm's intensification. For quantitative size measurements, a transparent acetate sheet with a square grid of known size was placed on a magnified image of the brain region of interest. The images were acquired with an Olympus BHS system microscope equipped with a Panasonic WV-CL500 video camera. A count was made of all grid intersections, or points, lying within the cross-sectional area of the structure of interest. The volume of the structure was calculated by multiplying this area measure by slice thickness. Although this work did not concentrate on a bilateral comparison, it found no significant difference between right and left antennal lobe volumes in 4-day-old ($n = 6$), 6-day-old ($n = 4$), or 28-day-old ($n = 6$) bees.

The first study explicitly devoted to the search for volumetric lateralization was performed by Rigosi et al. in 2011 [82] using two-photon microscopy. The fluorescent marker RH795 was bath-applied to the brain, and imaging was performed in vivo using an Ultima IV two-photon microscope (Prairie Technologies, Bruker) in combination with an ultra-short pulsed laser (Mai Tai Deep See HP, Spectra-Physics). The dye was excited at 1040 nm with an average laser power of 10 mW at the sample. An Olympus 40×, NA = 0.8 water-immersion objective provided a field of view width of approximately 300 μm. Volumetric measurements were obtained by collecting image stacks in steps of 3 μm along the anteroposterior axis. The imaging depth was limited to approximately 150 μm by the diffusion depth of the bath-applied dye. After 3D image reconstruction and segmentation (Fig. 8), no significant asymmetry in glomerular volumes was found in a subset of five glomeruli averaged over nine animals.

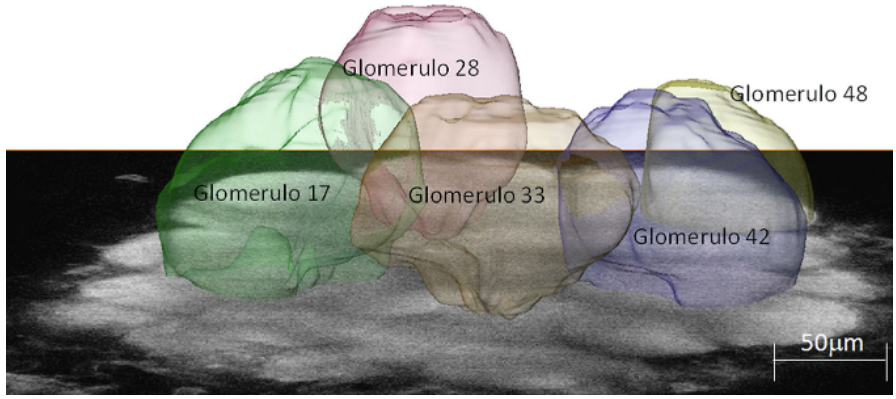

Fig. 8 Single image of the left antennal lobe of *Apis mellifera* at an imaging depth of approximately 80 µm, superimposed with the reconstructed 3D images of five glomeruli. (Reprinted from [82], copyright 2011, with permission from Elsevier)

Sensilla Imaging

The first evidence of structural lateralization in the honeybee nervous system has been obtained in the periphery of the olfactory system. Insects'antennae are covered by sensilla, porous cuticular structures of various morphology containing a variable number of olfactory sensory neurons. Via scanning electron microscopy, the authors identified and counted the different types of sensilla, detecting an asymmetry between the left and right antennae [1]. The mean number of sensilla placodea was significantly higher on the right antenna. In addition, bees learned significantly better when only the right antenna was available than with only the left antenna, suggesting a correlation between sensilla number and learning performance. Both anatomical and behavioral results were later confirmed by Frasnelli et al. [108]. In addition, performing SEM imaging, they reported that the asymmetry for non-olfactory sensilla was the opposite, and they were more frequent on the left antenna (Fig. 9). Similar results were found in *Bombus terrestris*, where the number of olfactory sensilla trichodea type A was significantly higher on the right antenna and, again, the odor leaning performance strongly depended on the involvement of the right antenna [109].

3.4.2 Fruit Fly

Standard Atlas of the Antennal Lobe

The first atlas of the *Drosophila* antennal lobe was produced by Stocker et al. in 1983 using a bright-field microscope [110]. Samples were prepared in vivo via local injections of cobalt chloride into the antennae. After imaging more than 400 cobalt-stained preparations, 19 glomeruli could be identified regarding their location, shape, and size in each antennal lobe. By staining only single antennas, glomeruli were characterized according to their ipsi- or bilateral input. By localized injections to flagellar regions bearing only a single type of sensillum, it was possible to observe similar

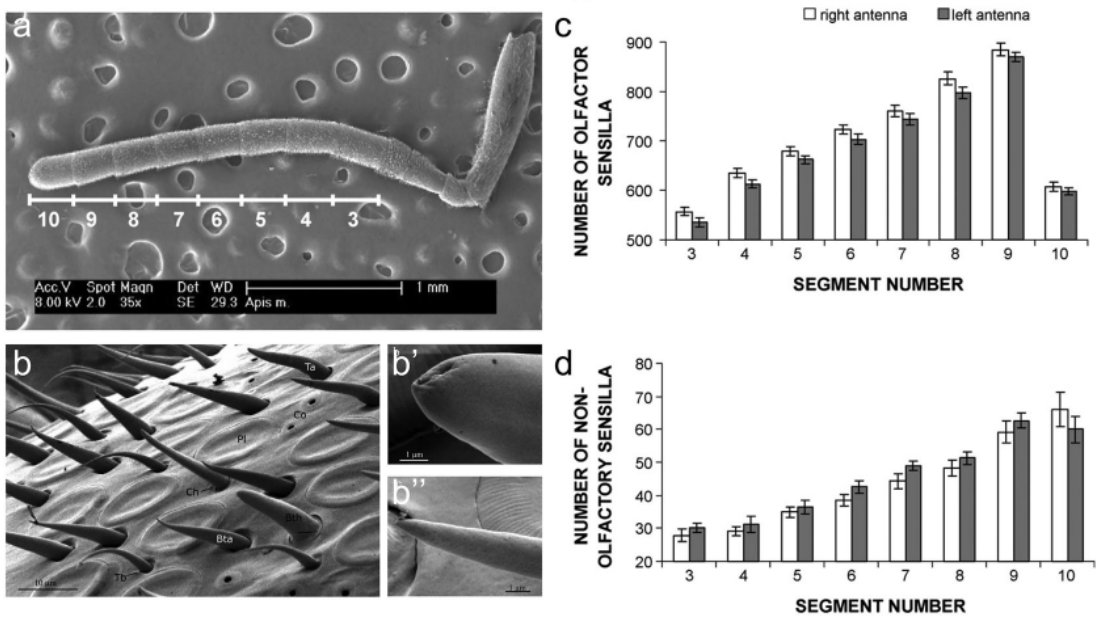

Fig. 9 Low-magnification SEM images, (**a**) ventral view of the *Apis mellifera* left antenna. (**b**) dorsal view of a medial segment of the flagellum with detail of a sensillum chaeticum (**b'**) and of a sensillum basiconicum (**b''**). (**c**, **d**) Count of the mean number of olfactory (**c**) and non-olfactory (**d**) sensilla on the right (*white*) and left (*grey*) antenna (± standard error) as a function of the segment number. (Reprinted from [108], with permission from Elsevier)

patterns of glomerular projections. These patterns reflected the sensillum type rather than its location on the antenna, which suggested that individual glomeruli received stereotyped olfactory inputs and might represent functional units.

The first full 3D brain atlas was created by Laissue and colleagues in 1999 [111] by performing nc82 antibody labeling in whole-mount preparation. Images were acquired with a confocal microscope at 3 images/μm interval with 512 × 512 pixel resolution, resulting in an average of 140 images per AL. Eight representative brains were processed for 3D analysis and reference brain reconstruction. This study confirmed the presence of the previously described glomeruli and revealed the existence of 8 new ones. Also, the higher staining quality and imaging resolution allowed better discrimination of glomerular boundaries and observation of glomerular compartments.

A systematic study of the expression of different olfactory receptor types was conducted by Couto et al. in 2005 [112]. This analysis confirmed previous anatomical results and provided further insight into the anatomical and functional organization of the AL. By constructing a set of mCD8-GFP reporter lines for all 62 odorant receptor promoters, the authors were able to localize reliably and identify all olfactory receptor-expressing neurons and

confirm the general validity of the "one receptor-one glomerulus" principle. More recently, Tanaka and colleagues [113] exploited the GAL4 enhancer-trap system and identified 29 neuronal types associated with the antennal lobe. Morphological analysis of the neuronal arborization revealed novel information about the organization of the local inter-glomerular network, providing a base for further morpho-functional studies of odor processing.

Dissection and fixation procedures cause strong volumetric and geometrical modifications of the fly brain, resulting in unpredictable deformation of the AL glomeruli and making it impossible to compare directly in vitro and in vivo images of the brains. Only recently, Grabe and colleagues [16] produced the first in vivo digital 3D atlas of the *Drosophila* AL. Transgenic flies expressing the red fluorescent protein DsRed directly fused to the presynaptic protein n-synaptobrevin, under the control of the pan-neuronal promoter *elav*, allowed genetic staining of the AL in the living animal. Optical sectioning was performed with a confocal microscopy equipped with a 40× water-immersion objective, and individual glomeruli were reconstructed using the segmentation software AMIRA. This approach provided a highly reliable topology of the antennal lobe in vivo, a very valuable tool for glomerular identification during functional imaging analysis.

Brain Asymmetries

One of the few studies on fly brain lateralization was conducted by Pasqual and colleagues, who investigated the relationship between brain asymmetry and long-term memory [72]. They described an unknown asymmetrical structure in the *Drosophila* brain, positioned in the right hemisphere, and hence named asymmetrical body (AB). This structure was revealed by anti-fasciclin II (FasII) antibody staining, together with a Bodian counterstaining used to visualize surrounding nerve fibers. The analysis was conducted on paraffin-embedded brain samples, sectioned into 7 μm frontal sections, and inspected using bright-field microscopy. Subsequently, a group of fruit flies was trained for associative memory formation and tested for short-term (3 h), and long-term (4 days) memory retention. Good-learner and bad-learner flies were systematically stained with anti-fasII antibody, and imaged via confocal microscopy, revealing that the FasII-expressing structure is bilateral only in 7.6% of the wild-type population (Fig. 10). Moreover, they observed that short-term memory performance was independent of the presence of the asymmetrical body. However, four days after the associative training, memory scores in the flies with the asymmetrical brain were the same as in the short-term, whereas flies with the symmetrical brain showed no signs of long-term memory formation.

A recent study used genetic tools to investigate further the neural and molecular correlates of such brain asymmetry

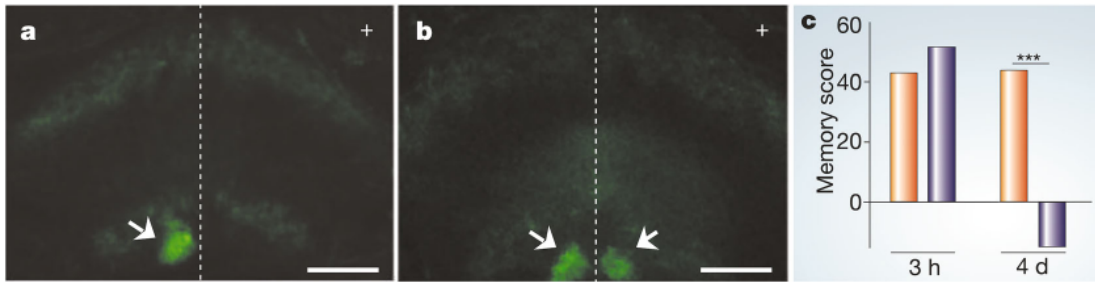

Fig. 10 Single confocal section showing the FasII-labelled asymmetrical body (arrow) in the majority of wild-type flies (**a**), while in a few flies the same structure presents a bilateral symmetry (**b**), scale bar 20 μm. (**c**) Learning performances measured 3 h and 4 days after conditioning show that brain lateralization strongly correlates with long-term memory. The orange bars represent flies with asymmetrical brains and the purple bars represent flies with symmetrical brains. (Reprinted by permission from Macmillan Publishers Ltd.: Nature [72], copyright (2005))

[114]. The study identified a set of bilateral cells, the H-neurons, which project their axons asymmetrically into the right AB in ~95% of the flies. Using the iRNA technique, Lapraz and colleagues revealed that the asymmetric innervation depends on the expression of netB, a ligand of the axon guidance receptor netrin. Moreover, behavioral tests on wild-type versus iRNA-treated flies revealed a fundamental role of the NetB pathways in building an asymmetrical neural circuit involved in long-term memory formation.

Asymmetries in the Larval Connectome

In 2023, the first connectome of an entire brain of the fly larva was generated from electron microscopy imaging [115]. A detailed analysis of the brain circuit architecture was performed by computer-assisted reconstruction with CATMAID (subheading "Electron Microscopy") in a nanometer-resolution EM volume of the central nervous system. This study resulted in the identification of 3016 neurons and 548,000 synapses. In this architecture, several signs of lateralization have been identified. Seven pairs of bilateral neurons had different postsynaptic partners on the ipsilateral and contralateral hemispheres, and 13 pairs only partially overlap between ipsilateral and contralateral targets. These neurons were suggested to be involved in controlling asymmetric motor patterns that require different subsets of muscles on the left and right sides of the body. The study also compared the number of synapses in neuron-to-neuron connections across hemispheres. In this case, asymmetries were found mostly in weakly connected neurons (1–2 synapses), while strong connections were highly conserved between hemispheres. Notably, the role of synaptic asymmetries still needs to be clarified.

3.4.3 Perspectives

Although a morphological asymmetry is apparent in fruit flies, no neuroanatomical lateralization has so far been detected in honeybees. However, relevant studies have been comparing brain regions on rather large scales. Thanks to modern fluorescence microscopy techniques, such as confocal, two-photon, and super-resolution imaging, the search for anatomical correlates of functional lateralization in the honeybee can be extended to single neurons and sub-cellular features. Single neuron staining will make it possible to quantitatively evaluate neuronal branching, while synaptic staining will provide measures for the synaptic density in different neuropils and across brain hemispheres. This will enable continuing the search for anatomical correlates of functional and behavioral lateralization on a new scale.

References

1. Letzkus P, Ribi WA, Wood JT et al (2006) Lateralization of olfaction in the honeybee *Apis mellifera*. Curr Biol 16:1471–1476. https://doi.org/10.1016/j.cub.2006.05.060
2. Kells AR, Goulson D (2001) Evidence for handedness in bumblebees. J Insect Behav 14:47–55. https://doi.org/10.1023/A:1007897512570
3. Vallortigara G, Rogers LJ, Bisazza A (1999) Possible evolutionary origins of cognitive brain lateralization. Brain Res Rev 30:164–175. https://doi.org/10.1016/S0165-0173(99)00012-0
4. Siniscalchi M (2013) Divided brains. The biology and behaviour of brain asymmetries, Cambridge
5. Rogers LJ (2015) Brain and behavioral lateralization in animals. Int Encycl Soc Behav Sci 4:799–805. https://doi.org/10.1016/B978-0-08-097086-8.53082-7
6. Frasnelli E, Vallortigara G, Rogers LJ (2012) Left-right asymmetries of behaviour and nervous system in invertebrates. Neurosci Biobehav Rev 36:1273–1291. https://doi.org/10.1016/j.neubiorev.2012.02.006
7. Hodgkin AL, Huxley AF (1945) Resting and action potentials in single nerve fibres. J Physiol 104:176–195. https://doi.org/10.1113/jphysiol.1945.sp004114
8. Matsumoto SG, Hildebrand JG (1981) Olfactory mechanisms in the moth *Manduca sexta*: response characteristics and morphology of central neurons in the antennal lobes. Proc R Soc B Biol Sci 213:249–277. https://doi.org/10.1098/rspb.1981.0066
9. Lieke EE (1993) Optical recording of neuronal activity in the insect central nervous system: odorant coding by the antennal lobes of honeybees. Eur J Neurosci 5:49–55. https://doi.org/10.1111/j.1460-9568.1993.tb00204.x
10. Joerges J, Küttner A, Galizia CG, Menzel R (1997) Representations of odours and odour mixtures visualized in the honeybee brain. Nature 387:285–288. https://doi.org/10.1038/387285a0
11. Galizia CG, Sachse S, Rappert A, Menzel R (1999) The glomerular code for odor representation is species specific in the honeybee *Apis mellifera*. Nat Neurosci 2:473–478. https://doi.org/10.1038/8144
12. Galizia CG, Nägler K, Hölldobler B, Menzel R (1998) Odour coding is bilaterally symmetrical in the antennal lobes of honeybees (*Apis mellifera*). Eur J Neurosci 10:2964–2974. https://doi.org/10.1111/j.1460-9568.1998.00303.x
13. Haase A, Rigosi E, Frasnelli E et al (2011) A multimodal approach for tracing lateralisation along the olfactory pathway in the honeybee through electrophysiological recordings, morpho-functional imaging, and behavioural studies. Eur Biophys J 40:1247–1258. https://doi.org/10.1007/s00249-011-0748-6
14. Paoli M, Galizia GC (2021) Olfactory coding in honeybees. Cell Tissue Res 383:35–58. https://doi.org/10.1007/s00441-020-03385-5
15. Galizia CG, McIlwrath SL, Menzel R (1999) A digital 3-dimensional atlas of the honeybee antennal lobe based on optical sections